

₁ Study of neutrino-nucleus interaction at around 1 GeV using
₂ a 3D grid-structure neutrino detector, WAGASCI, muon
₃ range detectors and magnetized spectrometer, Baby MIND,
₄ at J-PARC neutrino monitor hall

₅ A. Bonnemaison, R. Cornat, L. Domine, O. Drapier, O. Ferreira, F. Gastaldi,
₆ M. Gonin, J. Imber, M. Licciardi, F. Magniette, T. Mueller, L. Vignoli, and O. Volcy
₇ *Ecole Polytechnique, IN2P3-CNRS, Laboratoire Leprince-Ringuet, Palaiseau,*
₈ *France*

₉ S. Cao and T. Kobayashi

₁₀ *High Energy Accelerator Research Organization (KEK), Tsukuba, Ibaraki, Japan*

₁₁ M. Khabibullin, A. Khotjantsev, A. Kostin, Y. Kudenko, A. Mefodiev, O. Mineev,
₁₂ S. Suvorov, and N. Yershov

₁₃ *Institute for Nuclear Research of the Russian Academy of Sciences, Moscow, Russia*

₁₄ B. Quilain

₁₅ *Kavli Institute for the Physics and Mathematics of the Universe (WPI), The*
₁₆ *University of Tokyo Institutes for Advanced Study, University of Tokyo, Kashiwa,*
₁₇ *Chiba, Japan*

₁₈ T. Hayashino, A. Hiramoto, A.K. Ichikawa, K. Nakamura, T. Nakaya, K Yasutome,
₁₉ and K. Yoshida

₂₀ *Kyoto University, Department of Physics, Kyoto, Japan*

₂₁ Y. Azuma, J. Harada, T. Inoue, K. Kin, N. Kukita, S. Tanaka, Y. Seiya,
₂₂ K. Wakamatsu, and K. Yamamoto

₂₃ *Osaka City University, Department of Physics, Osaka, Japan*

24 A. Blondel, F. Cadoux, Y. Favere, E. Noah, L. Nicola, and S. Parsa

25 *University of Geneva, Section de Physique, DPNC, Geneva, Switzerland*

26 N. Chikuma, F. Hosomi, T. Koga, R. Tamura, and M. Yokoyama

27 *University of Tokyo, Department of Physics, Tokyo, Japan*

28 Y. Hayato

29 *University of Tokyo, Institute for Cosmic Ray Research, Kamioka Observatory,*
30 *Kamioka, Japan*

31 Y. Asada, K. Matsushita, A. Minamino, K. Okamoto, and D. Yamaguchi

32 *Yokohama National University, Faculty of Engineering, Yokohama, Japan*

33 December 14, 2017

34 **Contents**

35	1	Introduction	3
36	2	Experimental Setup	4
37	2.1	Wagasci modules	5
38	2.1.1	Main detector	5
39	2.1.2	Electronics	8
40	2.1.3	Water system	9
41	2.2	INGRID Proton module	10
42	2.3	Baby MIND	11
43	2.3.1	Magnet modules	11
44	2.3.2	Scintillator modules	12
45	2.3.3	Electronics	14
46	2.3.4	Pefromance check	16
47	2.4	Side muon range detector	16

48	3 Physics goals	18
49	3.1 Expected number of events	19
50	3.2 Pseudo-monochromatic beam by using different off-axis fluxes	19
51	3.3 Subjects Wagasci can contribute	21
52	4 Status of J-PARC T59 experiment	22
53	5 MC studies	23
54	5.1 Detector simulation	23
55	5.1.1 Detector geometry	24
56	5.1.2 Response of detector components	25
57	5.2 Track reconstruction	25
58	5.3 Event selection	25
59	5.4 Cross section measurements on water	29
60	5.4.1 Charged current cross section measurement	30
61	6 Standalone WAGASCI-module performances	30
62	6.1 Reconstruction algorithm	32
63	6.1.1 Description	32
64	6.1.2 Performances	34
65	6.2 Background subtraction: the water-out module	41
66	7 Schedule	44
67	8 Requests	44
68	8.1 Neutrino beam	44
69	8.2 Equipment request including power line	44
70	8.2.1 Baby MIND Equipment request including power line	45
71	9 Conclusion	45

72 **1 Introduction**

73 The understanding of neutrino-nucleus interactions in the 1 GeV energy region is critical
 74 for the success of accelerator-based neutrino oscillation experiments such as the T2K exper-
 75 iment. Complicated multi-body effects of nuclei render this understanding difficult. The
 76 T2K near detectors have been measuring these and significant progress has been achieved.
 77 However, the understanding is still limited. One of the big factors preventing from full
 78 understanding is the non-monochromatic neutrino beam spectrum. Measurements with
 79 different but some overlapping beam spectra would greatly benefit to resolve the contrib-
 80 ution from different neutrino energies. We, the Wagasci collaboration, proposes to study

the neutrino-nucleus interaction at the B2 floor of the neutrino monitor building, where different neutrino spectra can be obtained due to the different off-axis position. Our experimental setup contains 3D grid-structure plastic-scintillator detectors filled with water as the neutrino interaction target (Wagasci modules), two side- and one downstream- muon range detectors(MRD's). The 3D grid-structure and side-MRD's allows a measurement of wider-angle scattering than the T2K off-axis near detector (ND280). High water to scintillator material ratio enables the measurement of the neutrino interaction on water, which is highly desired for the T2K experiment because it's far detector, Super-Kamiokande, is composed of water. The MRD's consist of plastic scintillators and iron plates. The downstream-MRD, so called the Baby MIND detector, also works as a magnet and provides the charge identification capability as well as magnetic momentum measurement for high energy muons. The charge identification is essentially important to select antineutrino events in the antineutrino beam because contamination of the neutrino events is as high as 30%. Most of the detectors has been already constructed. The Wagasci modules have been commissioned as the J-PARC T59 experiment and the Baby MIND detector was commissioned at the CERN neutrino platform. Therefore, the collaboration will be ready to proceed to the physics data taking for the T2K beam time in January 2019. We will provide the cross sections of the charged current neutrino and antineutrino interactions on water with slightly higher neutrino energy than T2K ND280 with wide angler acceptance. When combined with ND280 measurements, our measurement would greatly improve the understanding of the neutrino interaction at around 1 GeV and contribute to reduce one of the most significant uncertainty of the T2K experiment.

2 Experimental Setup

Figure. 1 and 2 show a schematic view and a CAD drawing of the entire set of detectors. Central neutrino target detectors consist of two Wagasci modules and T2K INGRID proton module. Inside the Wagasci module, plastic scintillator bars are aligned as a 3D grid-like structure and spaces in the structure are filled with water for a water-in Wagasci module. T2K INGRID proton module is a full active neutrino target detector which is composed only with scintillator bars in its tracking region. The central detectors are surrounded by two side- and one downstream- muon range detectors(MRD's) The MRD's are used to select muon tracks from the charged-current (CC) interactions and to reject short tracks caused by neutral particles that originate mainly from neutrino interactions in material surrounding the central detector, like the walls of the detector hall, neutrons and gammas, or neutral-current (NC) interactions. The muon momentum can be reconstructed from its range inside the detector. The MRD's consist of plastic scintillators and iron plates. In addition, each of the iron plates of the downstream-MRD, so called the Baby MIND detector, is wound by a coil and can be magnetized. It provide the charge selection capability.

For all detectors, scintillation light in the scintillator bar is collected and transported

119 to a photodetector with a wavelength shifting fiber (WLS fiber). The light is read out by
120 a photodetector, Multi-Pixel Photon Counter (MPPC), attached to one end of the WLS
121 fiber. The signal from the MPPC is read out by the dedicated electronics developed for the
122 test experiment to enable bunch separation in the beam spill. The readout electronics is
123 triggered using the beam-timing signal from MR to synchronize to the beam. The beam-
124 timing signal is branched from those for T2K, and will not cause any effect on the T2K
125 data taking.

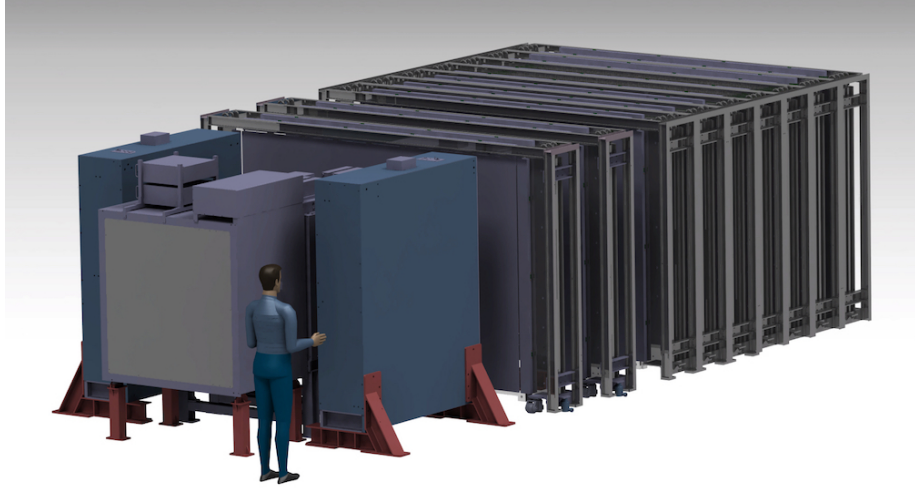


Figure 1: Schematic view of entire sets of detectors.

126 T2K adopted the off-axis beam method, in which the neutrino beam is intentionally
127 directed 2.5 degrees away from SK producing a narrow band ν_μ beam. The off-axis near
128 detector, ND280, is installed towards the SK direction in the B1 floor of the near detector
129 hall of the J-PARC neutrino beam-line. We propose to install our detector in the B2 floor
130 of the near detector hall, where the off-axis angle is similar but slightly different: 1.5 degree.
131 The candidate detector position in the B2 floor is shown in Fig. 3. The expected neutrino
132 energy spectrum at the candidate position is shown in Fig. 4.

133 2.1 Wagasci modules

134 2.1.1 Main detector

135 The WAGASCI modules are mainly composed of 1280 plastic scintillator bars and a sur-
136 rounding stainless steel tank as shown in Fig. 5. The total number of channels in one
137 Wagasci module is 1280. The stainless steel tank is constructed by welding stainless steel
138 plates, is sized as $46 \times 125 \times 125$ cm³, and weighs 0.5 ton.

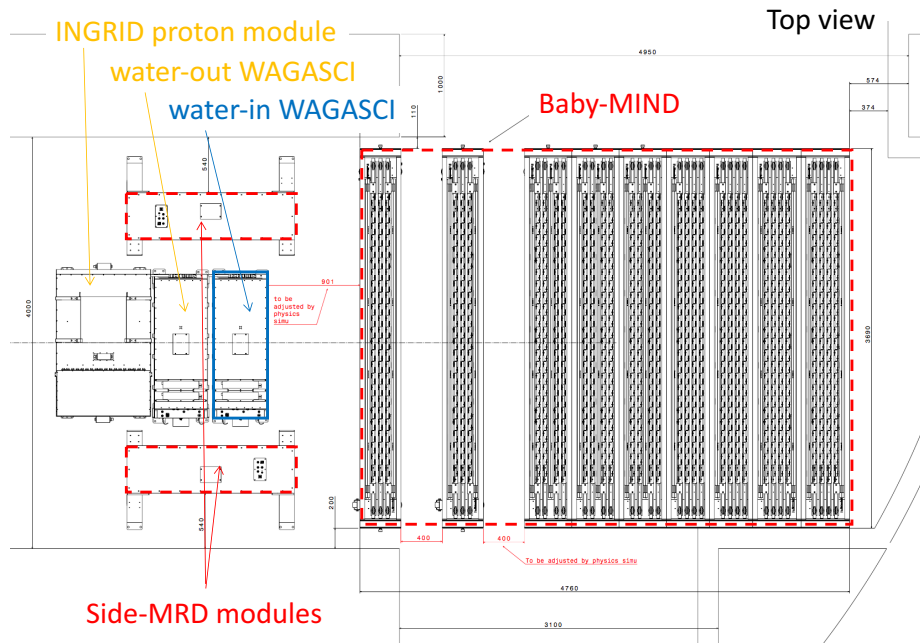


Figure 2: Top view of entire sets of detectors.

One Wagasci module consists of 16 scintillator tracking planes, where each plane is an array of 80 scintillator bars fixed with ABS frames. The 40 bars, called parallel scintillators, are placed perpendicularly to the beam, and the other 40 bars, called grid scintillators, are placed in parallel to the beam with grid structure in the tracking plane as shown in Fig. 5. Thanks to the 3 D grid-like structure of the scintillator bars, the Wagasci module has 4π angular acceptance for charged particles.

Thin plastic scintillator bars produced at Fermilab by extrusion method, mainly consists of polystyrene and are surrounded by thin reflector including TiO^2 (3 mm in thickness) are used for the Wagasci modules to reduce the mass ratio of scintillator bars to water, because neutrino interactions in the scintillator bars are a background for the cross section measurements on H_2O . Each scintillator bar is sized as $1020 \times 25 \times 3 \text{ mm}^3$ including the reflector part, and half of all the scintillator bars have 5-cm-interval slits to form the grid structure (Figure 6).

We will have two types of the Wagasci modules, a water-in module and a water-out module. The water-in Wagasci module has water in spaces of the grid structure. The total water mass serving as neutrino targets in the fiducial volume of the module is 188 kg, and the mass ratio of scintillator bars to water is 80 %. The water-out Wagasci module doesn't have water inside the detector. The total CH mass serving as neutrino target in the fiducial

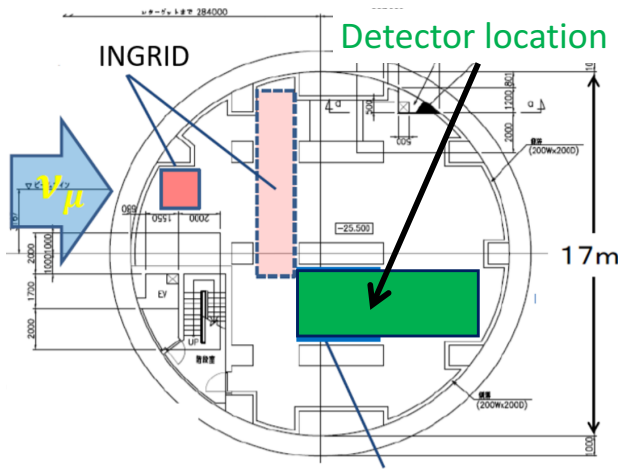


Figure 3: Candidate detector position in the B2 floor of the near detector hall.

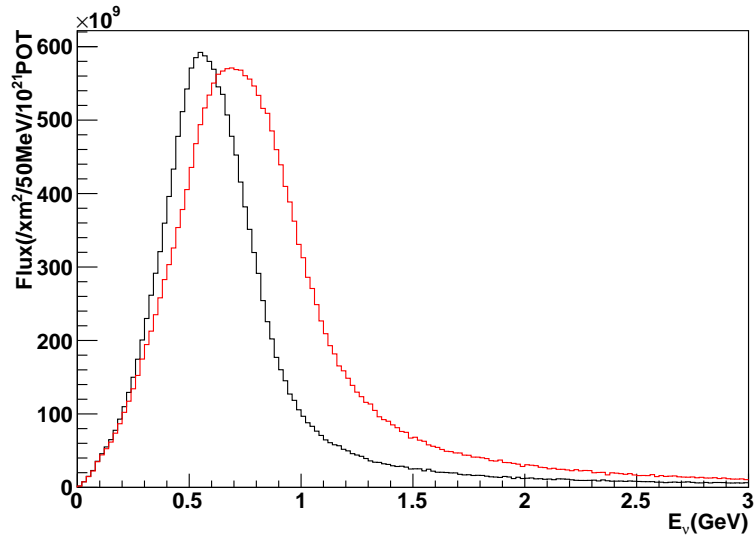


Figure 4: Neutrino energy spectrum at the candidate detector position (red, off-axis 1.5 degree). The spectrum at the ND280 site (black, off-axis 2.5 degree) is also shown.

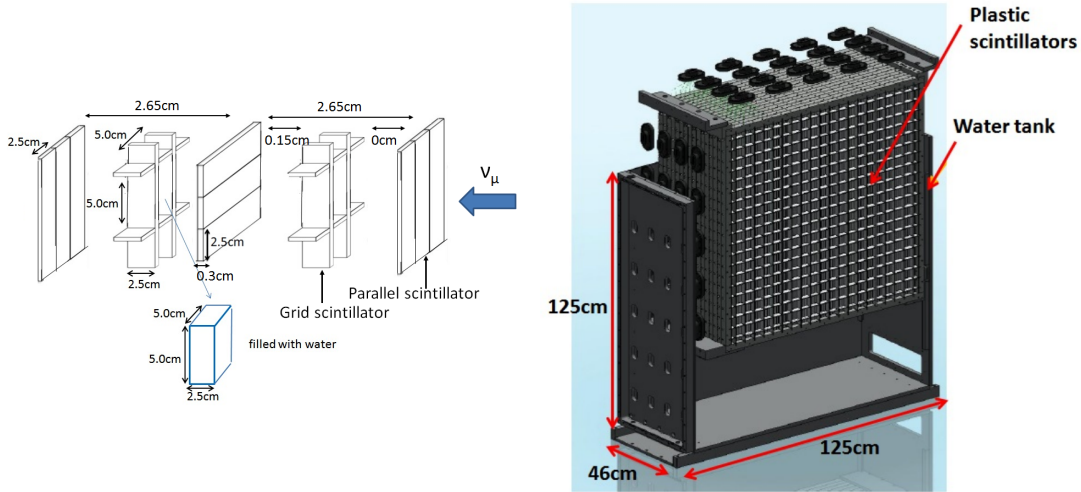


Figure 5: Schematic views of 3D grid-like structure of plastic scintillator bars (left) and Wagasci module (right).

157 volume of the module is 47 kg, and the mass fraction of scintillator bars is 100 %.

158 Scintillation light is collected by wave length shifting fibers, Y-11 (non-S type with a
 159 diameter of 1.0 mm produced by Kuraray. A fiber is glued by optical cement in a groove
 160 on surface of a scintillator bar. 32 fibers are gathered together by a fiber bundle at edge
 161 of the module, and lead scintillation light to a 32-channel arrayed MPPC. Since crosstalk
 162 of light yield due to reflection on the inner surface of each cell has been observed, all the
 163 scintillator bars are painted black by aqueous color spray. It is confirmed by measurements
 164 with cosmic rays that black painting on the surface of the scintillator bars suppresses this
 165 crosstalk so that no significant crosstalk effect is observed within uncertainty.

166 32-channel arrayed MPPCs, as shown in the Fig. 7, are used for the modules. The
 167 surface of the fiber bundle is polished and directly attached onto the 32-channel arrayed
 168 MPPCs. The positions of 32 fibers on the bundle are aligned to fit the channels of MPPCs.
 169 The MPPC is a product of Hamamatsu Photonics, S13660(ES1), with suppressed noise
 170 rate of ~ 6 kHz per channel at 0.5 p.e. threshold. For each MPPC channel, 716 pixels of
 171 APD are aligned in a shape of circle.

172 2.1.2 Electronics

173 As front-end electronics of this detector, a Silicon PM Integrated Read-Out Chip (SPIROC)
 174 [?] is adopted. SPIROC is a 36-channel auto-triggered front-end ASIC, and is produced
 175 by OMEGA/ IN2P3. It not only contains an analog signal processing part such as amplifi-
 176 cation and shaping of the waveform, but contains a digital signal processing parts such as

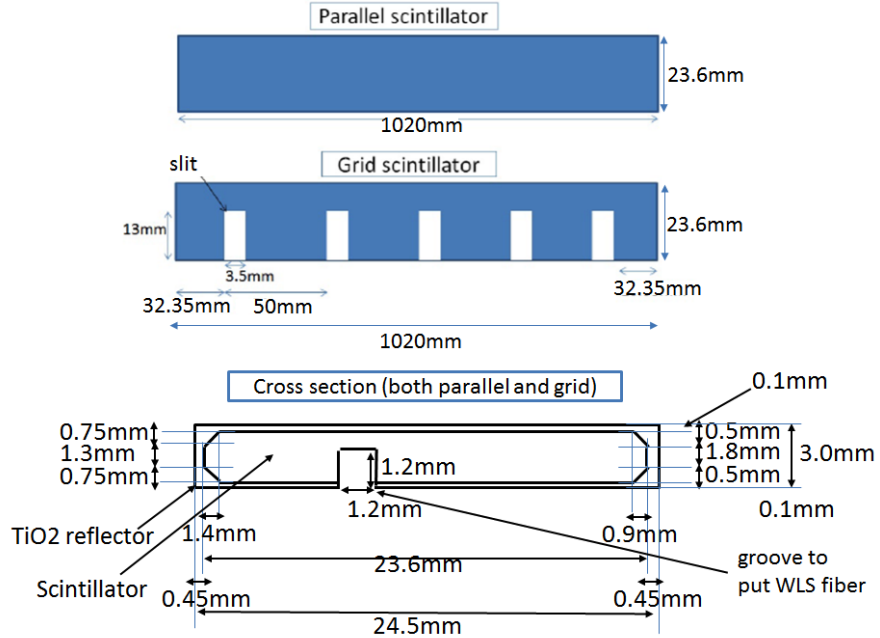


Figure 6: Geometry of scintillators used for Wagasci modules.

177 auto-trigger and timing measurement. Charge of MPPC signal is sampled by track-and-
 178 hold circuit. A Front-end electronics board, Active Sensor Unit (ASU), has been developed
 179 with the SPIROC2D chip, which is the latest version of SPIROC. Each readout board is
 180 designed to control a 32-channel arrayed MPPC, and 40 of the ASU boards are aligned on
 181 the module surface. The data acquisition system used for this detector, including back-end
 182 boards, has been developed for prototypes of ultra-granular calorimeters for the Interna-
 183 tional Linear Collider (ILC) [?], and independent of the T2K DAQ system. To synchronize
 184 the DAQ system to J- PARC neutrino beam, pre-beam trigger and beam trigger are sent to
 185 the clock control card. The beam trigger signals are converted from optical signals to NIM
 186 signals at NIM module on the B2 floor. In addition, the information of spill number are
 187 delivered with 16-bit ECL level signals, and converted to an Ethernet frame by an FPGA
 188 evaluation board to be directly sent to the DAQ PC. The electronics readout scheme is
 189 shown in Fig. 8.

190 **2.1.3 Water system**

191 Pure water is filled to the water tank of the water-in Wagasci module as follows. First,
 192 the water storage tank located at the B2 floor of the NM pit is filled with water delivered
 193 from a water tap on the ground level through a long hose. Second, the water is pumped

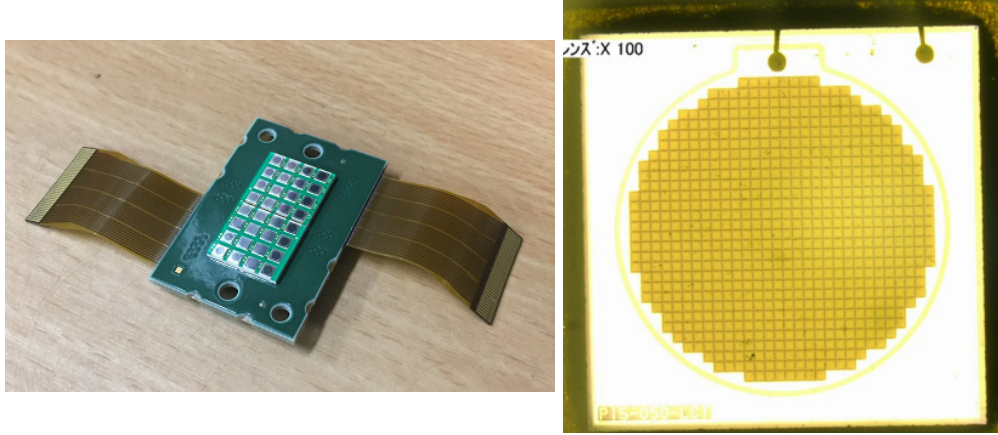


Figure 7: 32-channel arrayed MPPC (left) and an enlarged view of one MPPC channel (right).

194 to the other water storage tank though a water filler to produce pure water. Third, a
 195 compound preservative called Germall plus, which is the same preservative used in one of
 196 the sub-detectors of T2K ND280, FGD2, is put into the water to keep water from being
 197 bad. Then, the water is poured to the water-in Wagasci module, and it is kept in the
 198 module during the neutrino beam operation and not to be circulated.

199 **2.2 INGRID Proton module**

200 INGRID Proton module is a neutrino detectors of the T2K experiment. It is a fully-active
 201 tracking detector which consists of only scintillator strips. The purpose of this Proton
 202 Module is to separate the neutrino interaction types by detecting the protons and pions
 203 together with the muons from the neutrino interactions, and to measure the neutrino cross
 204 section for each interaction type. It consists of 36 tracking planes surrounded by veto planes
 205 (Figure 9), where each tracking plane is an array of two types of scintillator strips. The
 206 16 strips in the inner region have dimensions of $2.5\text{cm} \times 1.3\text{cm} \times 120\text{cm}$, while the 16 strips
 207 in the outer region have dimensions of $5\text{cm} \times 1\text{cm} \times 120\text{cm}$, making a plane of $120 \times 120\text{cm}^2$
 208 in the horizontal and vertical directions. The former is the scintillator produced for the
 209 K2K SciBar detector [3] and the latter was produced for INGRID. The tracking planes are
 210 placed perpendicular to the beam axis at 23mm intervals. Since the strips are aligned in one
 211 direction, each tracking plane is sensitive to either the horizontal or vertical position of the
 212 tracks. The tracking planes are therefore placed alternating in the horizontal and vertical
 213 directions so that three-dimensional tracks can be reconstructed. The tracking planes also
 214 serve as the neutrino interaction target. As with the Wagasci modules, scintillation light
 215 is read out by a WLS fiber and MPPC.

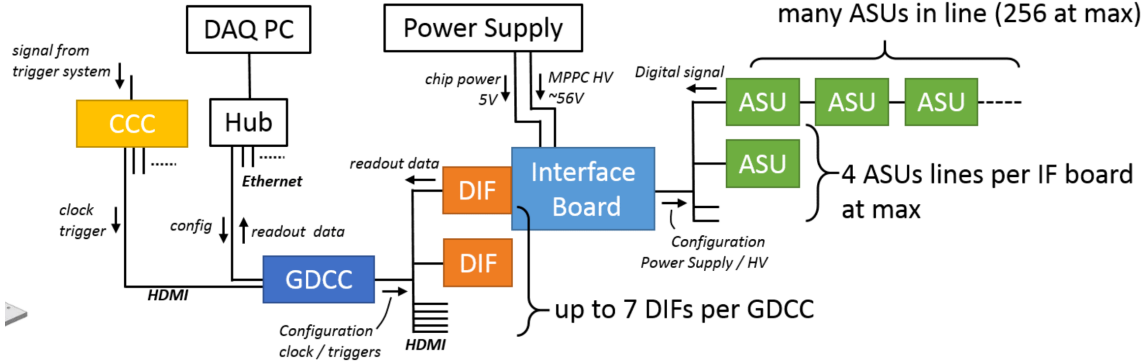


Figure 8: Wagasci electronics readout scheme.

216 It was installed at the neutrino beam axis on the SS floor of the T2K near detector hall
 217 in 2010, and had been used for neutrino cross section measurements. In August 2017, it
 218 was moved to the B2 floor of the T2K near detector hall by J-PARC T59 after getting the
 219 approval from T2K to use them. J-PARC T59 is performing a neutrino beam measurement
 220 using the detector from October 2017, and the measurement will continue until May 2018
 221 as we will discuss in Sec. 4.

222 2.3 Baby MIND

223 The Baby MIND is the downstream Muon Range Detector. It also works as a magnet and
 224 provides the charge identification capability as well as magnetic momentum measurement
 225 for high energy muons.

226 The Baby MIND collaboration ¹ submitted a proposal to the SPSC at CERN, SPSC-P-
 227 353. The project was approved by the CERN research board as Neutrino Platform project
 228 NP05 and constructed. The detector consists of 33 magnet modules, each 3500 mm ×
 229 2000 mm × 50 mm (30 mm steel) with a mass of approximately 2 tonnes. Of these magnet
 230 modules, 18 are instrumented with plastic scintillator modules.

231 2.3.1 Magnet modules

232 The Baby MIND is built from sheets of iron interleaved with scintillator detector modules
 233 but unlike traditional layouts for magnetized iron neutrino detectors (e.g. MINOS) which
 234 tend to be monolithic blocks with a unique pitch between consecutive steel segments and
 235 large conductor coils threaded around the whole magnet volume, the Baby MIND iron
 236 segments are all individually magnetized as shown in Fig. 10, allowing for far greater

¹Contact person: E. Noah, Spokesperson: A. Blondel, Deputy spokesperson: Y. Kudenko

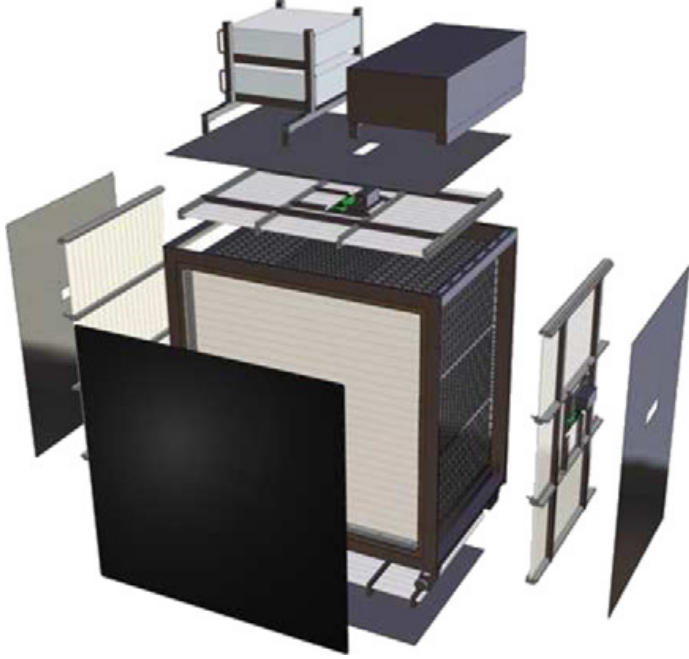


Figure 9: Schematic view of INGRID Proton module.

flexibility in the setting of the pitch between segments, and in the allowable geometries that these detectors can take.

The key design outcome is a highly optimized magnetic field map. A double-slit configuration for coil winding was adopted to increase the area over which the magnetic flux lines are homogeneous in B_x across the central tracking region. Simulations show the magnet field map to be very uniform over this central tracking region covering an area of $2800 \times 2000 \text{ mm}^2$, Fig. 11. The B_x component dominates in this region, with negligible B_y and B_z . This was confirmed by measuring the field with 9 pick-up coils wound around the first module. Subsequent modules were equipped with one pick-up coil. Test results on the 33 modules show all to achieve the required field of 1.5 T for a current of 140 A, with a total power consumption of 11.5 kW. The polarity of the field map shown in Fig. 11 (middle) can be reversed by changing the power supply configuration.

2.3.2 Scintillator modules

Each of the 18 scintillator modules is constructed from 2 planes of horizontal counters (95 counters in total) and 2 planes of vertical counters (16 counters in total) [2], arranged with an overlap between planes to achieve close to 100% hit efficiency for minimum ionizing muons. The arrangement of planes within a module is vertical-horizontal-horizontal-

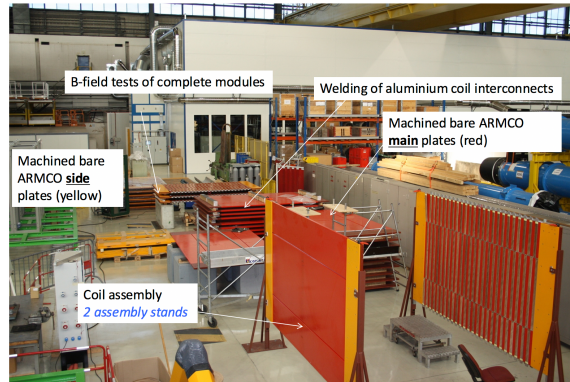


Figure 10: Magnet assembly zone at CERN.

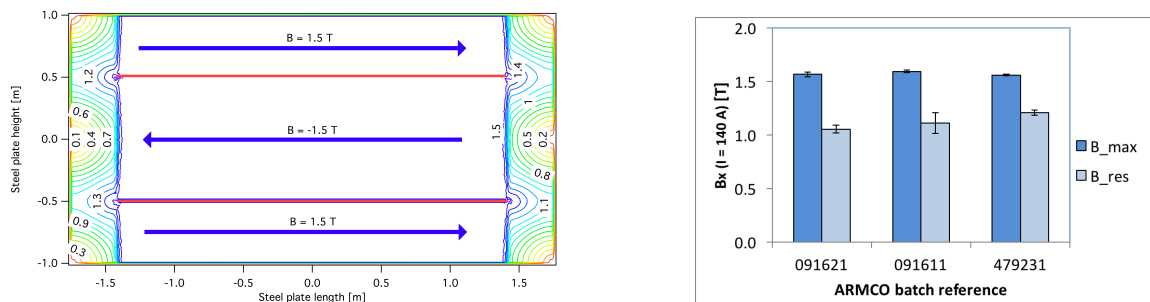


Figure 11: Left) Magnetic field map with a coil along 280 cm of the length of the plate. Right) Measured B field for 33 modules.

254 vertical. This arrangement was the result of an assembly approach whereby each plane
255 was built from 2 half-planes, with each half plane consisting of a horizontal plane and a
256 vertical plane. The scintillator bars are held in place using structural ladders that align
257 and maintain the counters, Fig. 12. No glue is used in the process, so counters can be
258 replaced. Aluminum sheets front and back provide light tightness.



Figure 12: Scintillator modules assembly. Left) top of front half-module showing vertical counters, and the spacers-ladders that set the pitch between horizontal counters and hold them in place. Middle) rear half-module showing horizontal counters on their ladders. Right) Assembled rear half-module, the front half-module can be seen in the background.

259 The plastic scintillator counters were made from 220 mm-wide slabs, consisting of
260 extruded polystyrene doped with 1.5% paraterphenyl (PTP) and 0.01% POPOP. They were
261 cut to size then covered with a 30-100 μm thick diffuse reflector resulting from etching of
262 the surface with a chemical agent [6, 7]. The horizontal counter size is $2880 \times 31 \times 7.5 \text{ mm}^3$,
263 with one groove along the length of the bar in which sits a wavelength shifting fiber from
264 Kuraray. The vertical counter size is $1950 \times 210 \times 7.5 \text{ mm}^3$, with one U-shaped groove
265 along the bar. On each counter, two custom connectors house silicon photomultipliers,
266 MPPC type S12571-025C from Hamamatsu, either side of the horizontal counter, and
267 both connectors at the top for the vertical counter. This geometrical configuration for
268 vertical counters was chosen for ease of connectivity to the electronics, and maintenance
269 operations.

270 A total of 1744 horizontal counters and 315 vertical counters (including spares) were
271 produced at the Uniplast company (Vladimir, Russia).

272 **2.3.3 Electronics**

273 The Baby MIND electronic readout scheme includes several custom-designed boards [8].
274 The revised version is shown in Fig. 13. At the heart of the system is the electronics
275 Front End Board (FEB), developed by the University of Geneva. The readout system
276 includes two ancillary boards, the Backplane, and the Master Clock Board (MCB) whose
277 development has been managed by INRNE (Bulgarian Academy of Sciences) collaborators.

278 The FEBv2 hosts 3 CITIROC chips that can each read in signals from 32 SiPMs [4].
279 Each signal input is processed by a high gain, and a separate low gain, signal path. The

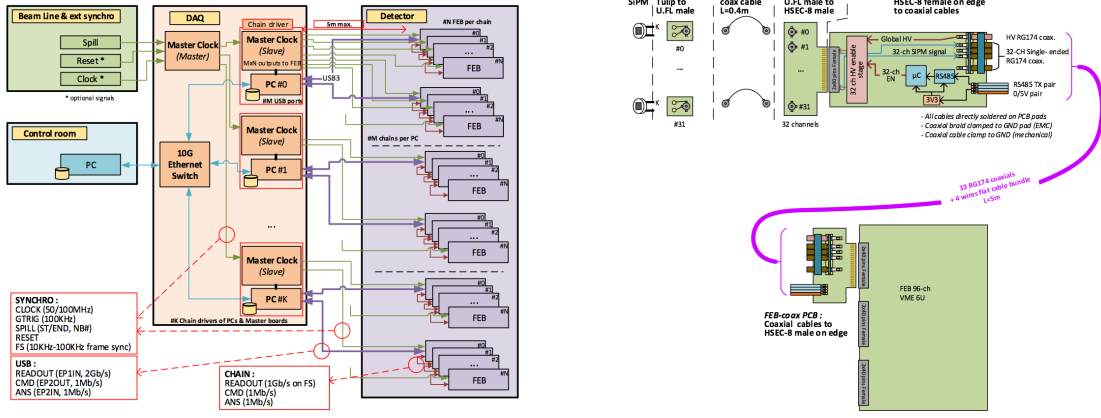


Figure 13: Left) Baby MIND electronics readout scheme. Right) SiPM-to-FEB connectivity.

outputs from the slow shapers can be sampled using one of two modes: a mode with an externally applied delay, and a peak detector mode. A faster shaper can be switched to either HG or LG paths, followed by discriminators with adjustable thresholds providing 32 individual trigger outputs and one OR32 trigger output. An Altera ARIA5 FPGA on the FEBv2 samples these trigger outputs at 400 MHz, recording rising and falling times for the individual triggers and assigning time stamps to these. Time-over-threshold from the difference between falling and rising times gives some measure of signal amplitude, used in addition to charge information and useful if there is more than one hit per bar within the deadtime due to the readout of the multiplexed charge output of $\sim 9 \mu\text{s}$. The ARIA5 also manages the digitization of the sampled CITIROC multiplexed HG and LG outputs via a 12-bit 8-ch ADC.

The internal 400 MHz clock on the FEBv2 can be synchronized to a common 100 MHz clock. The synchronization subsystem combines input signals from the beam line into a digital synchronization signal (SYNC) and produces a common detector clock (CLK) which can eventually be synchronised to an external experiment clock. Both SYNC and CLK signals are distributed to the FEBs. Tests show the FEB-to-FEB CLK(SYNC) delay difference to be 50 ps (70 ps). Signals from the beam line at WAGASCI include two separate timing signals, arriving 100 ms and 30 μs before the neutrino beam at the near detectors. The spill number is available as a 16-bit signal.

2.3.4 Pefromance check

All counters were measured at INR Moscow with a cosmic ray setup using the same type S12571-025C MPPCs and CAEN DT5742 digitizer. The average light yield (sum from both ends) was measured to be 37.5 photo-electrons (p.e.) per minimum ionizing particle (MIP)

303 and 65 p.e./MIP for vertical and horizontal counters, respectively. After shipment to
 304 CERN, all counters were tested once more individually with an LED test setup [?]. 0.1% of
 305 counters failed the LED tests and were therefore not used during the assembly of modules.
 306 The assembly of modules was completed in June 2017, and it was then tested in June and
 307 July 2017 at the Proton Synchrotron experimental hall at CERN with a mixed particle
 308 beam comprising mostly muons whose momenta could be selected between 0.5 and 5 GeV/c.
 An event display from the summer 2017 tests is shown in Fig. 14.

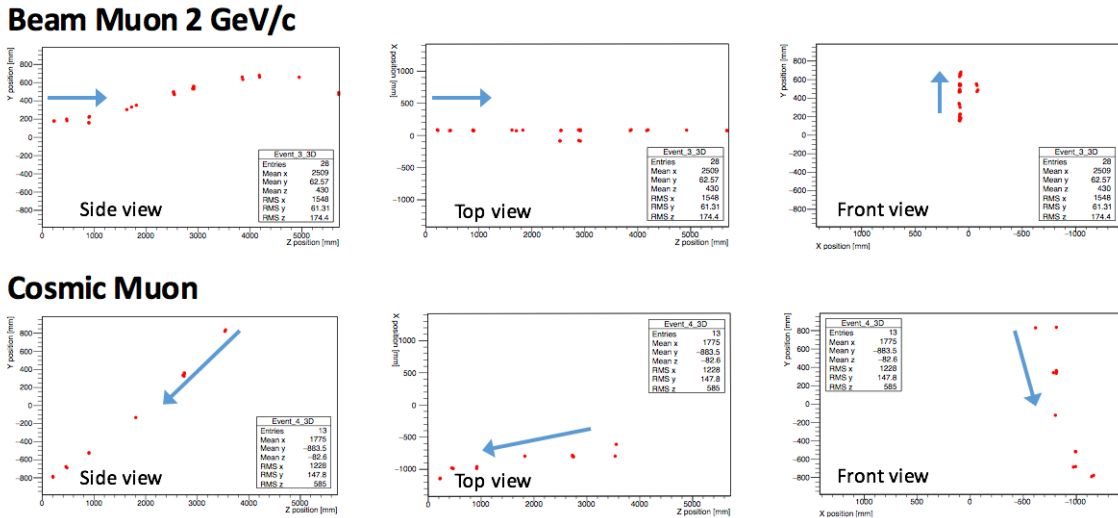


Figure 14: Comparison of a beam muon and cosmic muon in the three different geometrical projections of the detector. The beam impinges on the detector from the left. The arrows indicate the direction of travel of these muons. The direction of the cosmic muon is inferred from timing information.

309

310 2.4 Side muon range detector

311 Two Side-MRD modules for tracking secondary particles from neutrino interactions will be
 312 installed in 2018. Each Side-MRD module is composed of 11 steel plates and 10 layers of
 313 total 80 scintillator slabs installed in 13 mm gaps between the 30 mm thick plates. Each
 314 steel plate size is $30 \times 1610 \times 1800 \text{ mm}^3$. Total module size is $2236 \times 1630 \times 975 \text{ mm}^3$ as
 315 shown in Fig. 15 (left), weight is ~ 8.5 ton.

316 Scintillator bars were manufactured by Uniplast company in Vladimir, Russia. Polystyrene
 317 based scintillators were extruded with thickness of 7 mm, then cut to the size of $7 \times 200 \times$
 318 1800 mm^3 . Dopant composition is 1.5% PTP and 0.01% POPOP. Scintillator surface was
 319 etched by a chemical agent to form a white diffuse layer with excellent reflective perfor-
 320 mance. Ideal contact between the scintillator and the reflector raises the light yield up to

321 50% comparing to an uncovered scintillator. Sine like groove was milled along the scin-
 322 tillator to provide uniform light collection over the whole scintillator surface. WLS Y11
 323 Kuraray fiber of 1 mm diameter is glued with an optical cement EJ-500 in the S-shape
 324 groove as shown in Fig. 15(right). Bending radius is fixed to 30 mm that was specified to
 325 be safe for Kuraray S-type fibers. Both ends of the fiber are glued into optical connectors
 326 which mounted within a scintillator body and provide an interface to SiPMs, Hamamatsu
 327 MPPC S13081-050CS(X1).

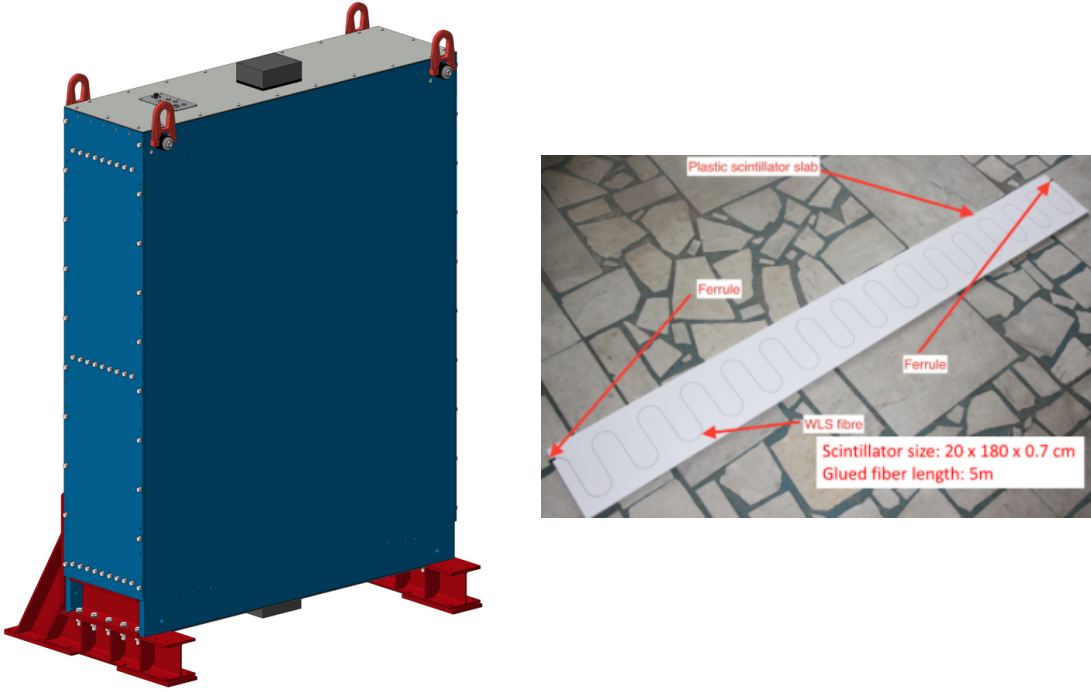


Figure 15: Left :Side-MRD module. Right: Scintillator bar of the Side-MRD modules.

328 Scintillators for the Side-MRD modules had been assembled at INR in Russia, and
 329 shipped to Japan in July 2017. The light yield for each scintillator was measured with
 330 cosmic rays at INR and at YNU in Japan after delivery. Parameters measured at the
 331 center of the counter were : the light yields LY_1 and LY_2 at both ends, the light yield
 332 asymmetry between the ends calculated as $100\% \times \frac{LY_1 - LY_2}{LY_1 + LY_2}$. After tests at INR we selected
 324 counters from measured 332 ones with the mean light yield of 45 p.e./MIP ($LY_1 + LY_2$
 334) and the asymmetry value less than 10 % . The measuremens at YNU yielded the average
 335 total light yield of about 40 p.e./MIP which varies in range from 32 to 50 p.e./MIP (Fig.
 336 16 (left)). Only two counters showed relatively high asymmetry close to 25 % as shown in

337 Fig. 16 (right). Using the results of the quality assurance test we selected 320 scintillator
338 counters for the Side-MRD modules.

339 We also measured the time resolution for a combination of four counters piled each on
340 another one. The average result for four counters is $\sigma_T = 1.04$ ns. The resolution of com-
341 bination of 2, 3, 4 counters is measured to be 0.79 ns, 0.66 ns and 0.58 ns, correspondently.

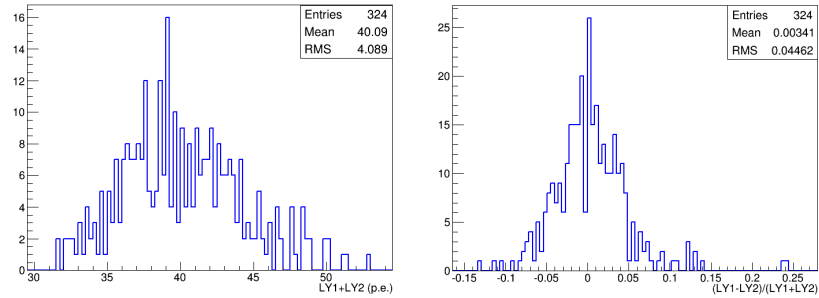


Figure 16: Total light yield distribution (left) and light yield assymetry (right) measured at YNU.

342
343 Construction of Side-MRD modules will be done from November 2017 at Yokohama
344 National University, then they will be transported to J-PARC and will be installed at B2
345 floor of the T2K near detector hall.

346 3 Physics goals

347 We will measure the differential cross section for the charged current interaction on H_2O
348 and Hydrocarbon(CH)). The water-scintillator mass ratio of the Wagasci module is as
349 high as 5:1 and the high purity measurement of the cross section on H_2O is possible. One
350 experimental option is to remove water from one of the two Wagasci modules. The water-
351 out WAGASCI module will allow to measure pure-CH target interactions with very low
352 momentum-threshold for protons. It will also benefit to subtract the background from
353 interaction with scintillator in the water target measurement. Another option is to add
354 the T2K proton module which is fully made of plastic scintillators. It will allow the high
355 statistics comparison of cross section between H_2O and CH and also comparison with
356 the ND280 measurement. The actual configuration will be optimized with detailed MC
357 simulation by 2018 Summer.

358 Our setup allows the measurements of inclusive and also exclusive channels such as $1-\mu$,
359 $1-\mu 1p$, $1-\mu 1\pi \pm np$ samples, former two of which are mainly caused by the quasi-elastic and
360 2p2h interaction and the latter is mainly caused by resonant or coherent pion production

and deep elastic scattering. In general, an accelerator produced neutrino beam spectrum is wide and the energy reconstruction somehow rely on the neutrino interaction model. Therefore, recent neutrino cross section measurement results including those from T2K are given as a flux-integrated cross section rather than cross sections as a function of the neutrino energy to avoid the model dependency. We can provide the flux-averaged cross section. In addition, by combining our measurements with those at ND280, model-independent extraction of the cross section for narrow energy region becomes possible. This method was demonstrated in [1] and also proposed by P** (NUPRISM).

3.1 Expected number of events

Expected number of neutrino events after the event selections is evaluated with Monte Carlo simulations as we will discuss in Section 5. In the neutrino-mode, 4.2×10^3 , 1.1×10^3 and 3.8×10^3 CC neutrino events are expected in the water-in WAGASCI module, the water-out WAGASCI module and the INGRID proton module after the selections with 0.5×10^{21} POT, and its purities are 78.0 %, 97.5 % and $\sim 98\%$. In the antineutrino-mode, 1.7×10^3 , 0.4×10^3 and 1.5×10^3 CC antineutrino events are expected in the water-in WAGASCI module, the water-out WAGASCI module and the INGRID proton module after the selections with 0.5×10^{21} POT, and its purities are 59.5 %, 74.4 % and $\sim 74\%$.

Statistical errors of flux integrated CC-inclusive neutrino cross section measurements on H₂O (full acceptance) and CH targets (forward acceptance) will be 1.5 % and 1.6 % with 0.5×10^{21} POT in the neutrino-mode. Statistical errors of flux integrated CC-inclusive antineutrino cross section measurements on H₂O (full acceptance) and CH targets (forward acceptance) will be 2.4 % and 2.5 % with 0.5×10^{21} POT in the antineutrino-mode.

Statistical errors of flux integrated H₂O to CH CC-inclusive neutrino cross section ratio measurement will be 3.1 % (full acceptance) and 2.3 % (forward acceptance) with 0.5×10^{21} POT in the neutrino-mode. Statistical errors of flux integrated H₂O to CH CC-inclusive antineutrino cross section ratio measurement will be 5 % (full acceptance) and 3.7 % (forward acceptance) with 0.5×10^{21} POT in the antineutrino-mode.

3.2 Pseudo-monochromatic beam by using different off-axis fluxes

The off-axis method gives narrower neutrino spectrum, and the peak energy is lower for larger off-axis angle. There still remains high energy tail mainly due to neutrinos from Kaon decay. The off-axis angle of the Wagasci location is 1.5 degree and different from the ND280 2.5 degree. Top two plots of Fig. 17 show the energy spectra of fluxes and neutrino interaction events at these two different locations. The high energy tail of ND280 flux can be somehow subtraction by using the Wagasci measurement. The low energy part of the Wagasci flux can be also subtracted by using the ND280 measurement. Bottom two plots of Fig. 17 demonstrate this method. We can effectively get two fluxes, from 0.2 GeV to 0.9 GeV and 0.6 GeV and 2 GeV and measure flux-integrated cross section for these two

398 fluxes.

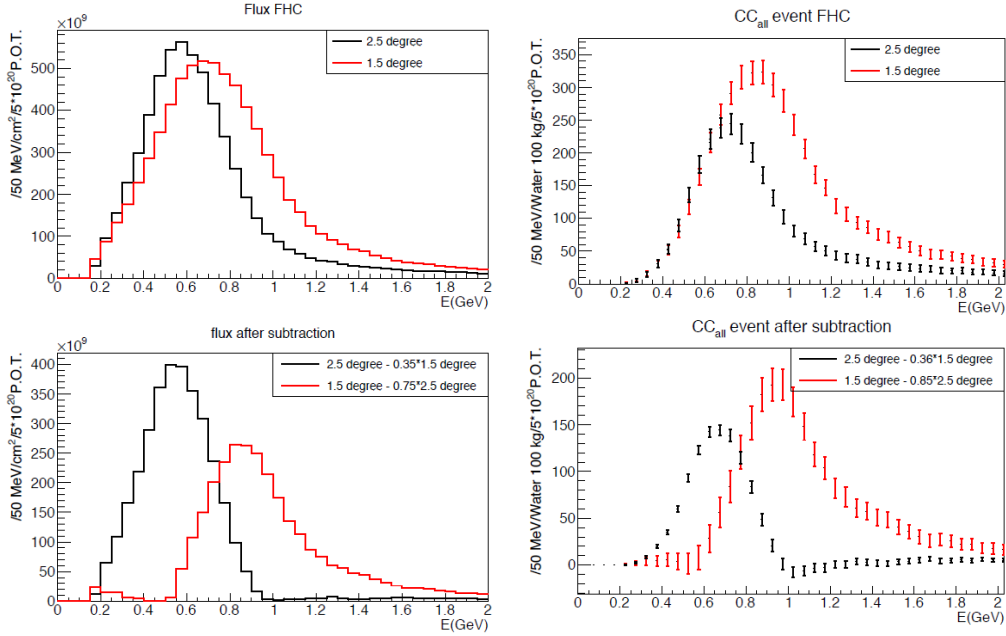


Figure 17: Energy spectra obtained by using different off-axis angle fluxes. Top two plots show the fluxes(left) and spectra of interaction events (right) for ND280 (off-axis 2.5 degree) and Wagasci (off-axis 1.5 degree). Bottom two plots show the fluxes (left) and spectra of interaction events (right) obtained by subtraction of fluxes at ND280 and Wagasci. The error bar is for the statistical error and those in the bottom right plot is obtained assuming the statistical error for ND280 measurement is much smaller than that of Wagasci experiment.

399 Statical errors of flux integrated CC-inclusive neutrino cross section measurements
400 on H₂O (forward acceptance) and CH targets (forward acceptance) with the pseudo-
401 monochromatic beam will be 2 % and 1.9 % with 0.5×10^{21} POT in the neutrino-mode.
402 Statical errors of flux integrated CC-inclusive antineutrino cross section measurements
403 on H₂O (forward acceptance) and CH targets (forward acceptance) with the pseudo-
404 monochromatic beam will be 3 % and 2.8 % with 0.5×10^{21} POT in the neutrino-mode.

405 3.3 Subjects Wagasci can contribute

406 In T2K experiment, neutrinos interact with bound nucleons in relatively heavy nuclei
407 (Carbon and Oxygen), so the cross-section is largely affected by nuclear effects. The nuclear
408 effects are categorized as nucleons' momentum distribution in nucleus, interactions with

409 correlated pairs of nucleons in nucleus (two particles-two holes, 2p2h), collective nuclear
410 effects calculated with Random Phase Approximation (RPA) and final state interactions
411 (FSI) of secondary particles in the nuclei after the initial neutrino interactions.

412 The 2p2h interactions mainly happen through Δ resonance interactions following a
413 pion-less decay and interactions with a correlated nucleon pair. The 2p2h interactions are
414 observed in electron scattering experiments [5] where the 2p2h events observed in the gap
415 between Quasi-Elastic region and Pion-production region as shown in Fig. 18. Neutrino
416 experiments also attempt to measure the 2p2h interactions, but separation of the QE peak
417 and the 2p2h peak is more difficult because transferred momentum (p) and energy (w)
418 are largely affected by neutrino energies which cannot be determined event-by-event in the
419 wide energy spectrum of the accelerator neutrino beam. Our model-independent narrow
420 neutrino spectra extracted from combined analyses of our data and ND280 data are ideal
421 for searching the 2p2h interaction because clearer separation of the QE peak and the 2p2h
422 peak is expected. Another way to observe the 2p2h interaction is direct measurement of
423 proton tracks in CC0 π sample with low detection threshold and full acceptance. Fig. 19
424 shows proton multiplicities after FSI in CCQE events and 2p2h events, and Fig. 20 shows
425 opening angles among two proton tracks in the same samples. The water-out Wagasci
426 can provide good sample for the 2p2h interaction search because its low density medium
427 enables the detection of low momentum protons in addition to the full acceptance.

428 The corrections from collective nuclear effects calculated by RPA as a function of Q^2 are
429 shown in Fig. ???. The Q^2 dependence of the correction can be tested by measuring angular
430 distribution of muons in CC1- μ and CC1- $\mu 1p$ events. The uncertainties of the corrections
431 in low (high) Q^2 regions can be constrained by observing the events with a forward-going
432 (high-angle) muon, so it is essential to measure muon tracks with full acceptance.

433 T2K experiment is starting to use ν_e CC1 π events for its CP violation search to increase
434 the statistics. One of the biggest uncertainty of the CC1 π sample comes from the final
435 state interactions of pions in the nuclei after the initial neutrino interactions because they
436 change the multiplicity, charge and kinematics of the pions. The multi-pion production
437 events can be migrated into the CC1 π sample due to the FSIs, and they become important
438 backgrounds. We can constrain the uncertainties from the pion FSIs by measuring pion
439 rescattering in the detector and pion multiplicity in ν_μ CCn π sample with low detection
440 threshold and full acceptance for pion tracks. The water-out WAGASCI can provide good
441 sample for the pion FSI studies because its low density medium enables the detection of
442 low momentum pions in addition to the full acceptance.

443 4 Status of J-PARC T59 experiment

444 We had submitted a proposal of a test experiment to J-PARC in April 2014 to test a new
445 detector with a water target, WAGASCI, at the neutrino monitor hall, and the proposal
446 was approved as J-PARC T59. The project contains the side and downstream muon range

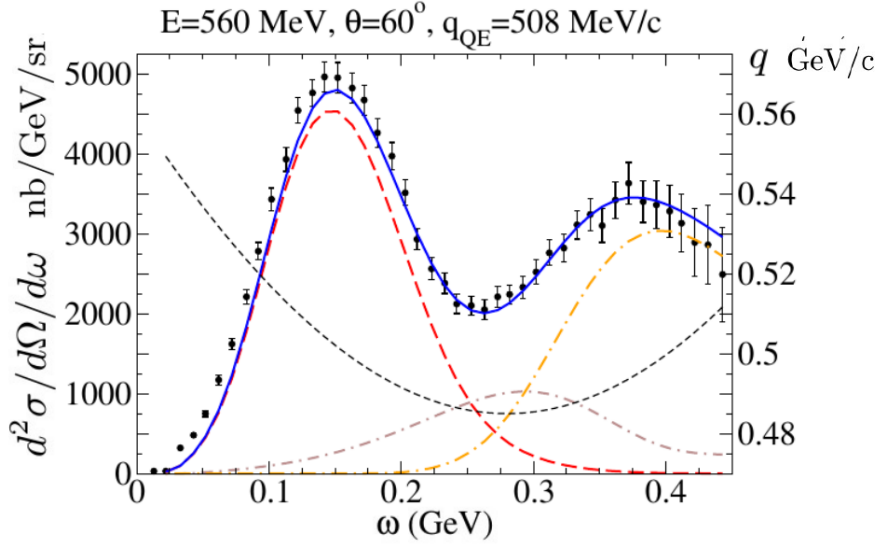


Figure 18: Comparison of inclusive $^{12}\text{C}(\text{e},\text{e}')$ cross sections and predictions of the QE-SuSAv2 model (long-dashed red line), 2p-2h MEC model (dot-dashed brown line) and inelastic-SuSAv2 model (long dot-dashed orange line) (from Ref. [5]). The sum of the three contributions is represented with a solid blue line. The q dependence with w is also shown (short-dashed black line.)

detectors as well.

The first WAGASCI module has been constructed in 2016 and installed at the on-axis position in front of the T2K INGRID detector for the commissioning and the first cross section measurement as a part of the T2K experiment. The INGRID electronics boards are used to read the signal. The light yield measured with muons produced by the interaction of neutrinos in the hall wall, shown in Fig. 21, is sufficiently high to get good hit efficiency. A track search algorithm based on the cellular automaton has been developed using the software tools by the T2K INGRID. Examples of observed events are shown in Fig. 22. The tracking efficiency in 2-dimensional projected plane was evaluated by comparing the reconstructed track in the WAGASCI module and the INGRID module and shown in Fig. 23. Note that the tracking efficiency for high angle (> 70 deg) is not evaluated because of the acceptance of the INGRID module, not because of the limitation of the WAGASCI module.

In 2017 Autumn, the construction of the second WAGASCI module and the dedicated electronics board were completed. The module and the electronics were installed to the B2 floor together with the T2K proton module and the INGRID module as shown in Fig. 24. The proton module is to be used as the entering muon veto and also for the comparison

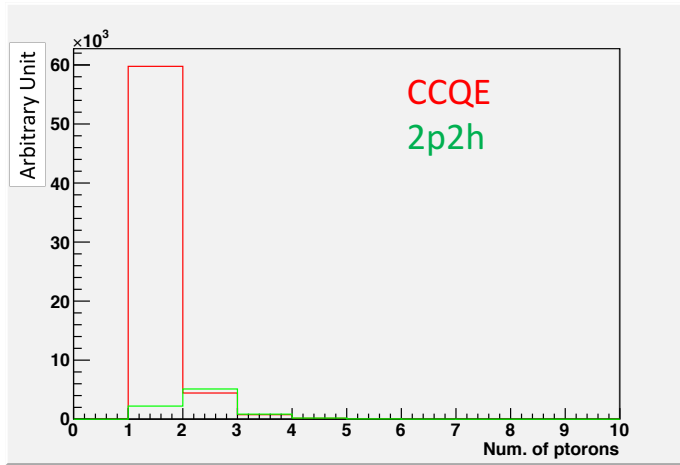


Figure 19: Proton multiplicities after FSI in CCQE events and 2p2h events.

464 of interaction between CH and Water. The INGRID module is for the temporary muon
 465 detector with limited acceptance for this period. The detector was commissioned and is
 466 in operation to take data with the antineutrino beam during the T2K beam time from
 467 October.

468 The production of the components of the side muon range detectors has been completed
 469 and now the detectors are being assembled at the Yokohama National University. These
 470 detectors will be installed sometime from January to June, 2018 when T2K is not running.

471 The Baby MIND detector was transported from CERN to Japan in December, 2017.
 472 It will be installed and commissioned in Jan.-Feb. 2018 and T59 will take the neutrino-
 473 induced muon data in April and May.

474 5 MC studies

475 5.1 Detector simulation

476 Expected number of neutrino events in the water-in Wagasci detector is evaluated with
 477 Monte Carlo simulations. Neutrino beam flux at the detector location is simulated by
 478 T2K neutrino flux generator, JNUBEAM, neutrino interactions with target materials are
 479 simulated by a neutrino interaction simulator, NEUT, detector responses are simulated
 480 using GEANT4-based simulation. The neutrino flux at the detector location, 1.5 degrees
 481 away from the J-PARC neutrino beam axis, is shown in Figure 4, and its mean neutrino
 482 energy is around 0.68 GeV.

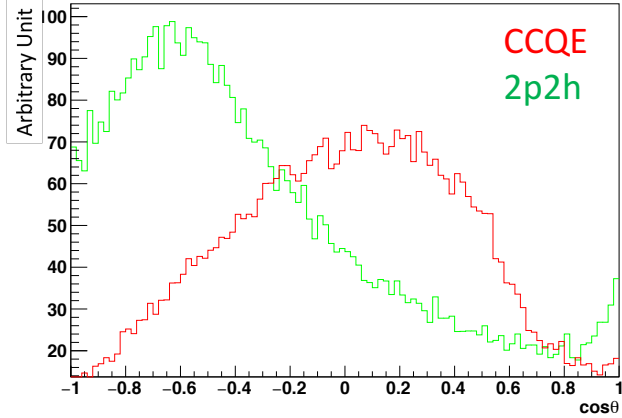


Figure 20: Opening angles among two proton tracks after FSI in CCQE events and 2p2h events.

483 5.1.1 Detector geometry

484 The detector geometry in the GEANT4-based simulation is slightly different from the actual
 485 detector as shown in Fig. 25. The active neutrino target region consists of four Wagasci
 486 modules, and each Wagasci detector has the dimension with $100\text{ cm} \times 100\text{ cm}$ in the x and
 487 y directions and 50 cm along the beam direction. Two Side-MRD modules are installed at
 488 both sides of the Wagasci modules, and each Side-MRD module consists of ten iron plates
 489 whose dimension is 3 cm (thickness) \times 200 cm (height) \times 320 cm (width). The distance
 490 between the Side-MRD modules and Wagasci modules is 80 cm. The downstream-MRD
 491 equivalent to the Baby-MIND is installed at the downstream of the Wagasci modules. The
 492 downstream-MRD consists of thirty iron plates whose dimension is 3 cm (thickness) \times 200
 493 cm (height) \times 400 cm (width). The distance between the downstream-MRD modules and
 494 Wagasci modules is 80 cm.

495 5.1.2 Response of detector components

496 The energy deposit inside the scintillator is converted into the number of photons. The
 497 effects of collection and attenuation of the light in the scintillator and the WLS fiber are
 498 simulated, and the MPPC response is also taken into account. The light yield is smeared
 499 according to statistical fluctuations and electrical noise.

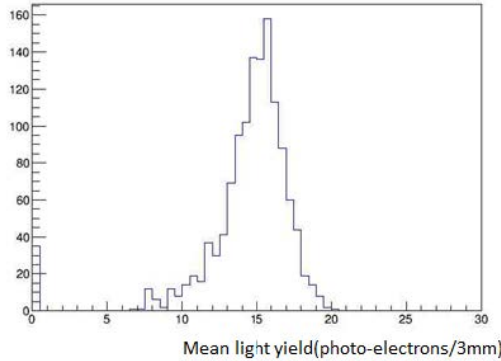


Figure 21: Light yield for muons produced by the interaction of neutrinos in the hall wall. Average light yields for each channel are plotted.

500 **5.2 Track reconstruction**

501 To select neutrino interaction from the hit patterns, a track reconstruction algorithm is
502 developed. The flow of the track reconstruction is as follows.

- 503 1. Two-dimensional track reconstruction in each sub-detectors
504 2. Track matching among the sub-detectors
505 3. Three -dimensional track reconstruction

506 Add explanation about two-dim reco, track matching and three-dim reco here.

507 **5.3 Event selection**

508 First, the events with the track which starts in 5 cm from the wall of the Wagasci module
509 are rejected to remove the background from the outside.

510 Second, to reject backgrounds from NC and neutral particles, the longest tracks are
511 required to penetrate more than one (five) iron plates in Side-MRD modules (Baby-MIND).
512 Then, in order to measure muon momentum, the longest tracks are required to stop in
513 MRDs (Side-MRD modules and Baby-MIND) or penetrate all iron plates.

514 Table 1 and 2 show numbers of the selected events in one water-in Wagasci module
515 after each event selection in neutrino-mode and antineutrino-mode respectively. As for
516 the neutrino-mode, 8478 CC events are expected with 1×10^{21} POT, and the purity is
517 78.0 %. The main background for the neutrino-mode is the neutrino interactions in the
518 scintillators inside the Wagasci detector. As for the antineutrino-mode, 3331 CC events
519 are expected with 1×10^{21} POT, and the purity is 59.5 %. The main background for the

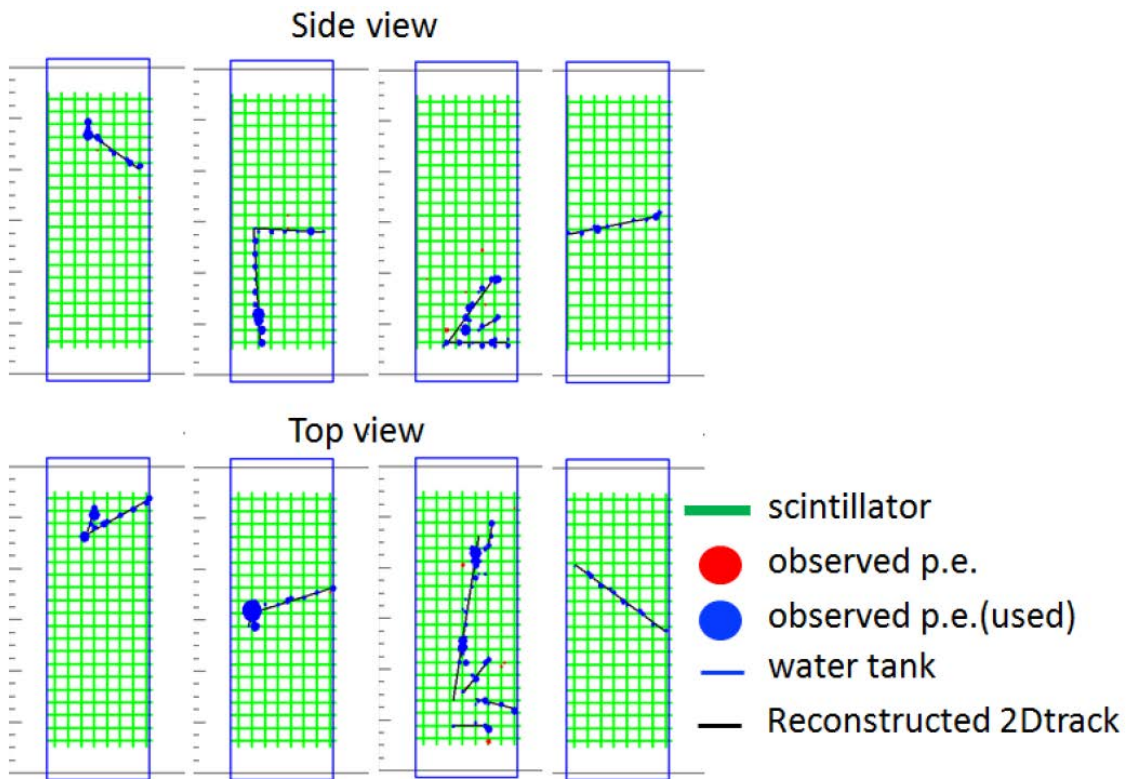


Figure 22: Example event displays of the WAGASCI module at on-axis. The reconstructed tracks are overlaid.

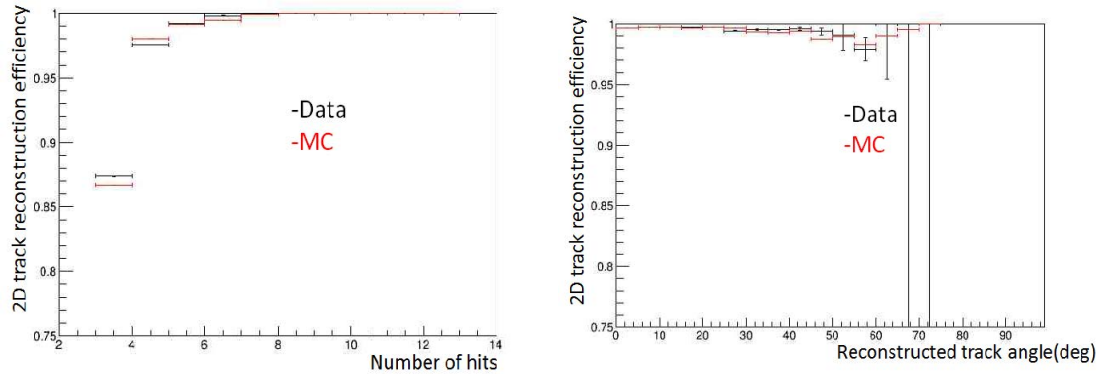


Figure 23: 2D track reconstruction efficiency as a function of number of hits (left) and track angle (right). Here the track angle is the one reconstructed by the INGRID module.

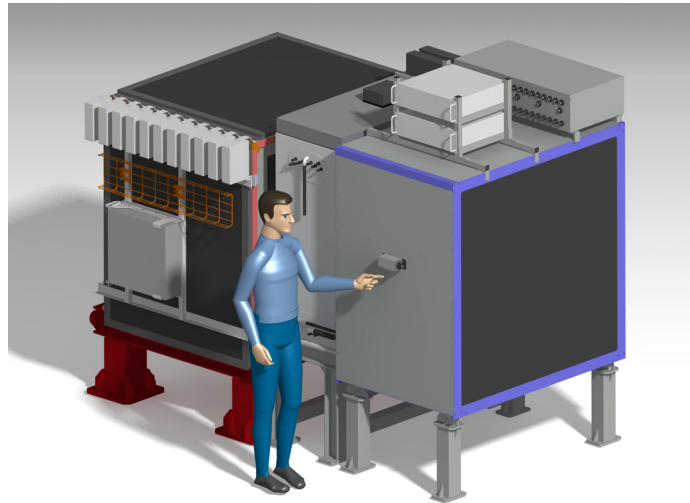


Figure 24: J-PARC T59 detector configuration in October 2017.

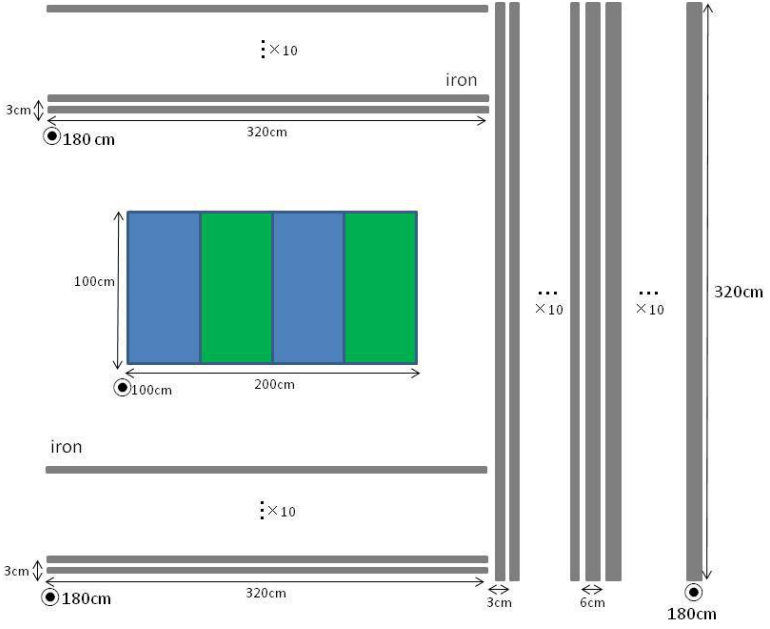


Figure 25: Geometry of the detectors in the Monte Carlo simulation.

antineutrino-mode is the wrong sign contamination from ν_μ events and the antineutrino interactions in the scintillators inside the Wagasci detector.

Table 3 and 4 show numbers of the charged-current events in the water-in Wagasci module after all event selection with a classification based on interactions at a vertex with 1×10^{21} POT in neutrino-mode and antineutrino-mode respectively.

Table 5 and 6 show numbers of the charged-current events in one water-in Wagasci module after all event selection with a classification based on particles after final state interactions with 1×10^{21} POT in neutrino-mode and antineutrino-mode respectively.

Figure 26 and 27 show the reconstructed angles of the longest tracks in the selected events in the neutrino-mode and the anti-neutrino mode respectively. Figure 28, 29 30 and 31 show the iron plane numbers in Side-MRD and Baby-MIND corresponding to the end points of the longest tracks in the selected events in the neutrino-mode and the anti-neutrino mode.

5.4 Cross section measurements on water

In the water target events, the background from interaction with scintillators has to be subtracted by using the measurement of the hydrocarbon target.

Table 1: Expected number of the neutrino-candidate events in one water-in Wagasci module with 1×10^{21} POT in neutrino-mode.

Cut	CC	NC	Scinti Bkg.	Total
Reconstructed	18093.2	699.7	4698.3	23491.2
FV	15150.8	588.4	3934.8	19673.9
Pene. iron	11264.3	237.3	2875.4	14377.0
Stop/Penetrate MRDs	8478.2	214.0	2173.1	10865.2
after all cuts	78.0 %	2.0 %	20.0 %	100 %

Table 2: Expected number of the antineutrino-candidate events in one water-in Wagasci module with 1×10^{21} POT in antineutrino-mode.

Cut	CC	NC	Scinti Bkg.	Wrong sign bkg	Total
Reconstructed	6499.7	107.3	2234.4	2330.8	11172.1
FV	5457.9	89.3	1873.5	1946.6	9367.1
Pene. iron	4172.3	30.8	1440.9	1560.6	7204.6
Stop/Penetrate MRDs	3331.5	28.5	1120.3	1121.2	5601.5
after all cuts	59.5 %	0.5 %	20.0 %	20.0 %	100 %

536 **5.4.1 Charged current cross section measurement**

537 **6 Standalone WAGASCI-module performances**

538 In the previous sections, the WAGASCI detector was studied using the Muon Range Detectors. In this section, the standalone abilities of WAGASCI module are presented. Using
 539 the WAGASCI configuration presented in Section 5, we have evaluated that only 7% of
 540 the muons will be stopped in one of the WAGASCI modules. THowever, this proportion
 541 increases to 53% for pions and 73% for protons produced by neutrino interactions at 1.5°
 542 off-axis. Figure 32 shows the momentum distribution of these daughter particles as well as
 543

Table 3: Expected number of the charged-current events in the water-in Wagasci module after the event selections with 1×10^{21} POT in neutrino-mode with a classification based on interactions at a vertex.

CCQE	MEC	CCRes	CCDIS	Total
3716.3	747.0	2081.3	1132.3	7676.9
48.4 %	9.7 %	27.1 %	14.7 %	100 %

Table 4: Expected number of the charged-current events in the water-in Wagasci module after the event selections with 1×10^{21} POT in antineutrino-mode with a classification based on interactions at a vertex.

CCQE	MEC	CCRes	CCDIS	Total
2522.0	362.8	765.8	765.8	4416.4
hline	57.1 %	8.2 %	17.3 %	17.3 %
				100 %

Table 5: Expected number of the charged-current events in one water-in Wagasci module after the event selections with 1×10^{21} POT in neutrino-mode with a classification based on particles after final state interactions.

CC0 π	CC1 π	CC2 π	CCn π	Total
5423.1	1684.3	242.9	701.1	8051.4
67.4 %	20.9 %	3.0 %	8.7 %	100 %

544 for the sub-sample stopped in one of the WAGASCI modules. Therefore, the study of the
 545 standalone abilities of the WAGASCI module in this section are dominantly motivated by:

- 546 • the accurate measurement of the neutrino interaction final states. Though most of the
 547 muons will be reconstructed and identified in the MRDs, the hadronic particles will
 548 predominantly stops in one WAGASCI module. One has therefore to rely exclusively
 549 on the WAGASCI module information alone to reconstruct, identify and measure the
 550 momentum of pions or protons.
- 551 • the coverage of the MRDs is not 4π . Using the WAGASCI module information can
 552 therefore help to constraint the particles that exits the WAGASCI module but do
 553 not geometrically enters any MRD.
- 554 • the particle identification of low momenta muons $p_\mu < 300$ MeV/c that will leave only
 555 few hits in the MRD. Using the WAGASCI module information will clearly enhance

Table 6: Expected number of the charged-current events in one water-in Wagasci module after the event selections with 1×10^{21} POT in antineutrino-mode with a classification based on particles after final state interactions.

CC0 π	CC1 π	CC2 π	CCn π	Total
2529.3	520.0	37.9	96.0	3183.2
79.5 %	16.3 %	1.2 %	3.0 %	100 %

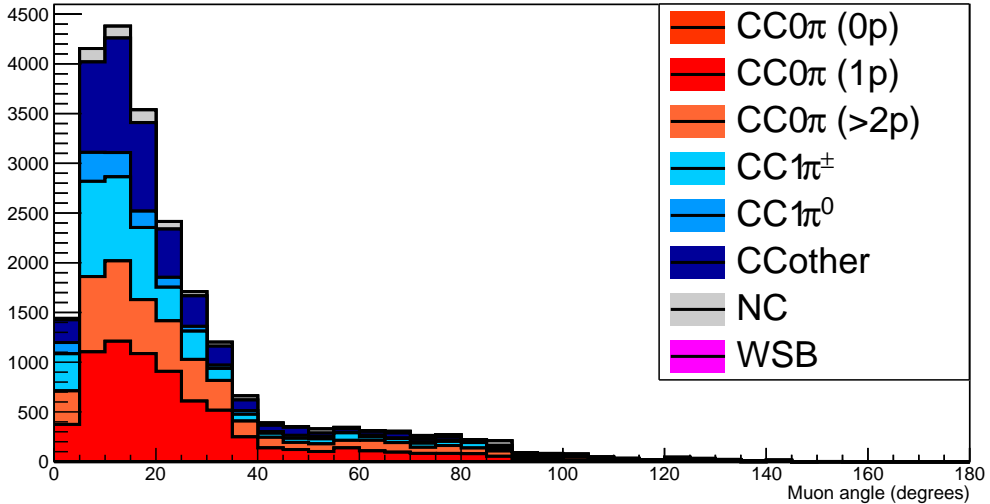


Figure 26: The reconstructed angles of the longest tracks in the selected events in the neutrino-mode.

556 the particle identification.

557 This study is based on an original study done for the ND280 upgrade target, with some
 558 modifications. Though the cell size is similar to the WAGASCI configuration presented
 559 in Section 5, the external dimensions are different ($186.4 \times 60 \times 130 \text{ cm}^3$). Whenever the
 560 results are presented with this external size and this parameter is likely to impact the
 561 result, it will be mentioned.

562 Note that in this section, a simplified reconstruction algorithm presented in Section 6.1 is
 563 used. The fiducial volume is chosen accordingly as the inner cube of the module which
 564 surfaces are distant of $4 \times$ scintillator space = 10 cm from the module external surfaces.

565 The neutrino interactions are simulated using NEUT v5.3.2. The NEUT input neutrino
 566 flux is estimated using JnuBeam v13a and assuming the detector to be located at 1.5°
 567 off-axis, as in Section 5. Note that the event reconstruction efficiency as a function of true
 568 neutrino energy might be changed at 1.5° , due for example to different Q^2 distributions. For
 569 this reason, one has to note that the reconstruction results might slightly be changed from
 570 2.5° and 1.5° . To avoid a similar change on the particle-only reconstruction efficiencies,
 571 they will be presented as a function of variables that completely characterize the particle
 572 kinematic state, *i.e.* its momentum and angle. Figure 33 shows the vertices distributions
 573 of the daughter particles of neutrinos interacting one standard WAGASCI water-module.

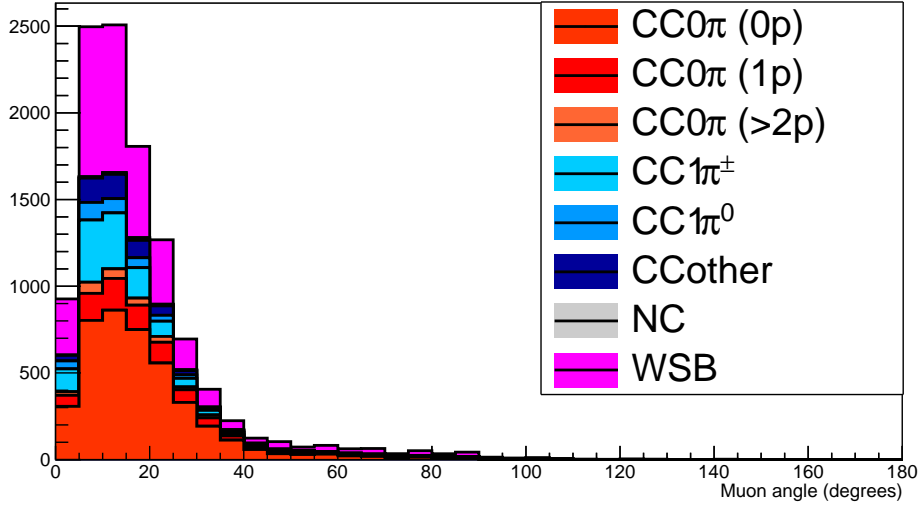


Figure 27: The reconstructed angles of the longest tracks in the selected events in the antineutrino-mode.

574 In this section, we will show the detector reconstruction and particle identification in this
 575 phase space, both for leptonic and hadronic particles. We will finally show an empty
 576 WAGASCI module can highly enhance the ability to constrain the neutrino interaction
 577 final state which is critical to reduce the corresponding uncertainties.

578 6.1 Reconstruction algorithm

579 6.1.1 Description

580 For this section, an ideal “simulated” reconstruction is developed. A particle is recon-
 581 structed if:

- 582 1. The particle is charged.
 583 2. Lets at least one hit (energy deposit > 2.5 photo-electron) in a scintillator.
 584

585 3. The particle enters one TPC and let one hit in the tracker.
 586 Or
 587

- 588 • The particle should be long enough to be reconstructed by the detector in at
 589 least 2 out of 3 views (XZ, YZ, XY). The length criterion requires the particle

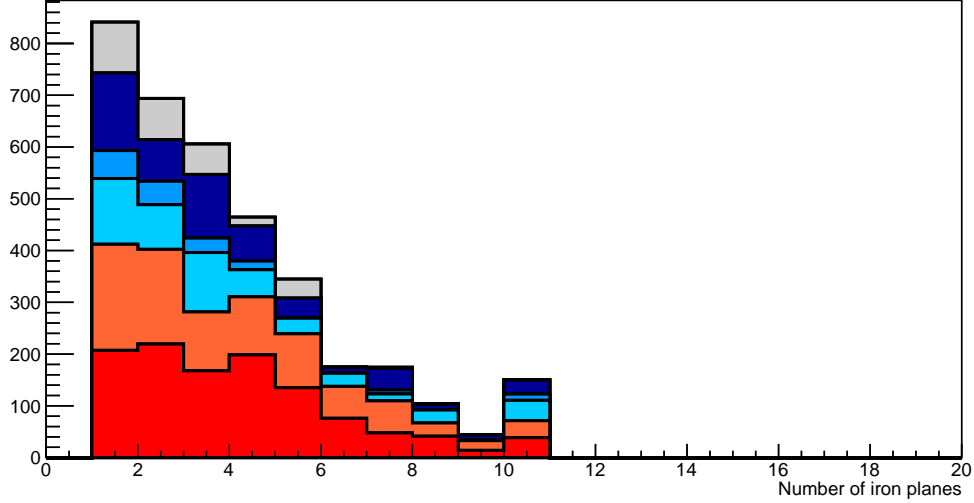


Figure 28: Iron plane numbers in Side-MRD corresponding to the end points of the longest tracks in the selected events in the neutrino-mode.

590
591
592

to let at least 4 hits in the detector. In the “less favourable case” of pure longitudinal or transverse going tracks, it represents a the track length of $L_{track} \geq 4 \times$ scintillator space = 10.0 cm.

593
594
595
596
597
598
599
600
601
602

- In the views where particles pass the length criterion, the particle shall not be superimposed with longer tracks in at least two views. The superposition criterion is estimated with the distance inter-tracks (DIT) which corresponds to the orthogonal distance between two tracks at the ending point of the shortest one (see Figure 34). For a track 1, the superposition criterion is tested with every longer tracks that starts at the same vertex. Let \vec{p}_1 the vector of track 1, and p_1^a its projections in the XZ, YZ and XY planes respectively for $i=1,2,3$. Note that these are projections in a 2D planes and not on a direction vector. In this case, the relative angle between the track 1 and a longer track 2 (of vector \vec{p}_2) in a view a is given by:

$$\cos \theta = \frac{\vec{p}_1^a \cdot \vec{p}_2^a}{\|\vec{p}_1^a\| \|\vec{p}_2^a\|} \quad (1)$$

603

and the distance inter track is given by:

$$DIT = \|\vec{p}_1^a\| \sin \theta \quad (2)$$

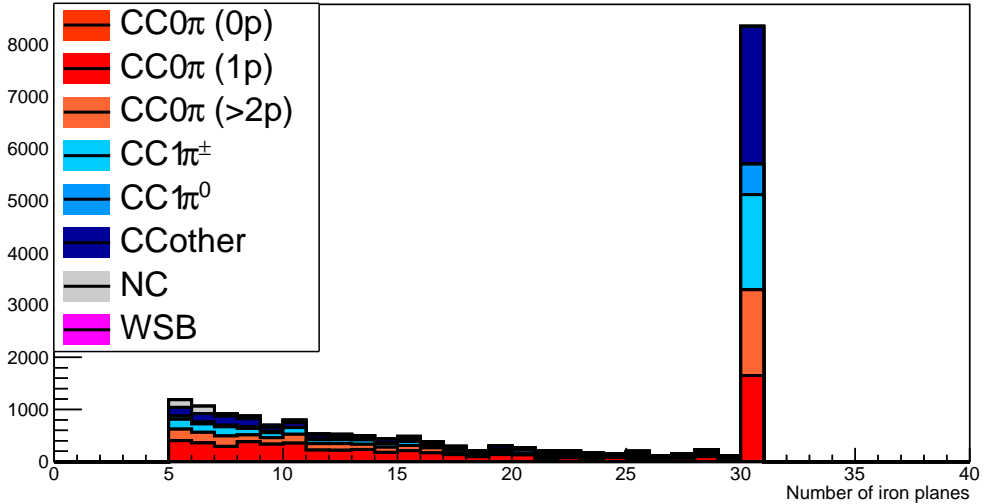


Figure 29: Iron plane numbers in Baby-MIND corresponding to the end points of the longest tracks in the selected events in the neutrino-mode.

604 The DIT should be higher than $4 \times$ scintillator width for the track 1 to be not
 605 superimposed with the track 2 in the view a, which also corresponds to 10.0 cm
 606 in the nominal configuration.

607 6.1.2 Performances

608 The particle-only reconstruction efficiencies and the reconstruction threshold in momenta
 609 are shown in Table 7. This threshold is defined as the maximal momentum for which the
 610 reconstruction efficiency is smaller than 30%. The thresholds in muon and pion momenta
 611 are 150 MeV/c. Most of the muons are above this threshold (see Figure 33) which leads
 612 to a 79% reconstruction efficiency.

613 The lower pion and proton efficiencies (respectively 52% and 26%) are due to lower
 614 efficiencies for similar momenta than muons, coming from strong interactions as shown
 615 on Figures 35. Efficiencies of each particle type tend to decrease in the backward region
 616 due to particle lower momenta. However, for a fixed momentum value, the reconstruc-
 617 tion efficiency is almost uniform which confirms the ability of the WAGASCI detector to
 618 reconstruct high angle tracks.

619 The reconstruction is thereafter tested on neutrino events. Table 8 summarizes the
 620 number of reconstructed events and efficiencies for each interaction type. As expected

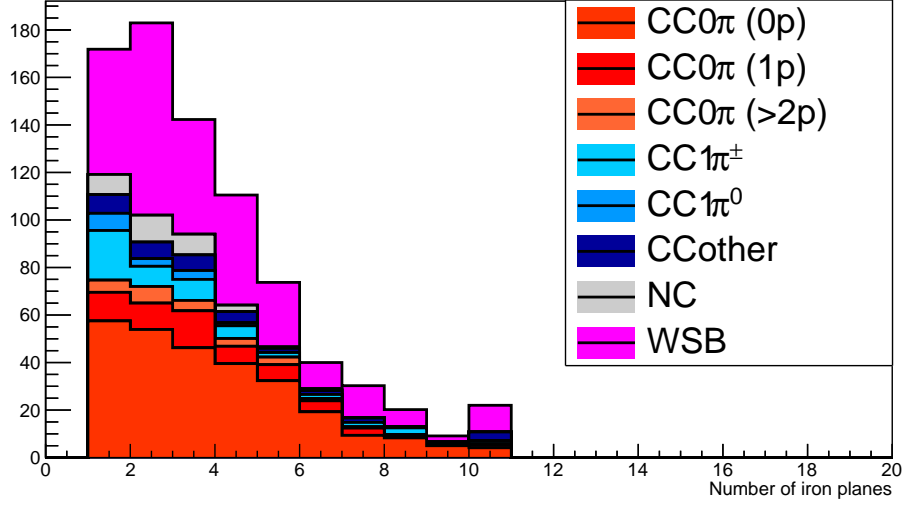


Figure 30: Iron plane numbers in Side-MRD corresponding to the end points of the longest tracks in the selected events in the antineutrino-mode.

	μ	π	p
Reconstruction Efficiency	79%	52%	26%
Momentum threshold	150 MeV/c	150 MeV/c	550 MeV/c

Table 7: Reconstruction efficiency and momentum threshold for muons, pions and protons. The threshold is defined as the maximal momentum for which particles have a reconstruction efficiency smaller than 30%.

from the high muon reconstruction efficiency, the charged current interactions have reconstruction efficiencies $\geq 85\%$.

The reconstruction efficiencies as a function of the neutrino energy and muon kinematics are respectively shown on Figure 36 and 37.

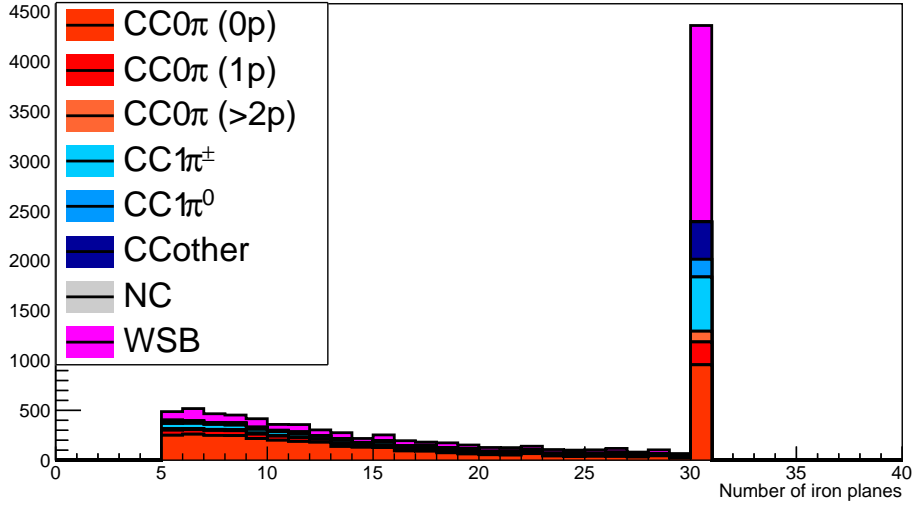


Figure 31: Iron plane numbers in Baby-MIND corresponding to the end points of the longest tracks in the selected events in the antineutrino-mode.

	CC0π	CC1π	CCOthers	NC	All
Reconstruction efficiency	85%	87%	91%	22%	68%

Table 8: Number of true interactions reconstructed. The purity and reconstruction efficiency of each true interaction is also shown.

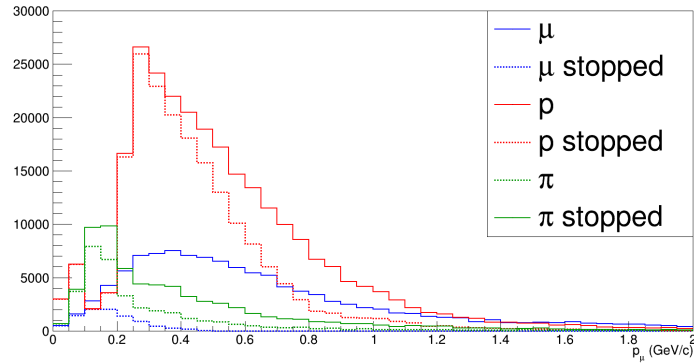


Figure 32: Momentum distribution of true particles in WAGASCI (plain) and corresponding distributions only for particles stopping into the WAGASCI module (dashed).

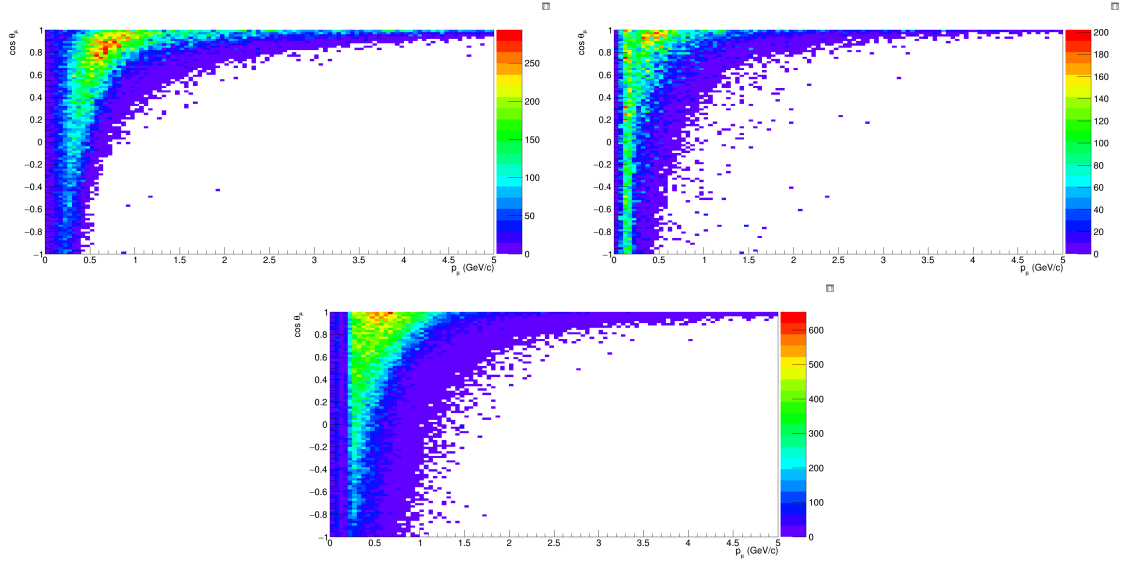


Figure 33: True number of muons (left), charged pions (right) and protons (bottom) in the two WAGASCI water-module as a function of the particles momenta and angles at 1.5° .

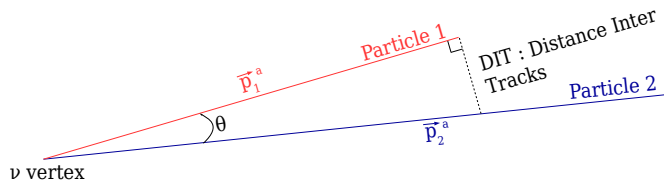


Figure 34: Definition of the distance inter tracks.

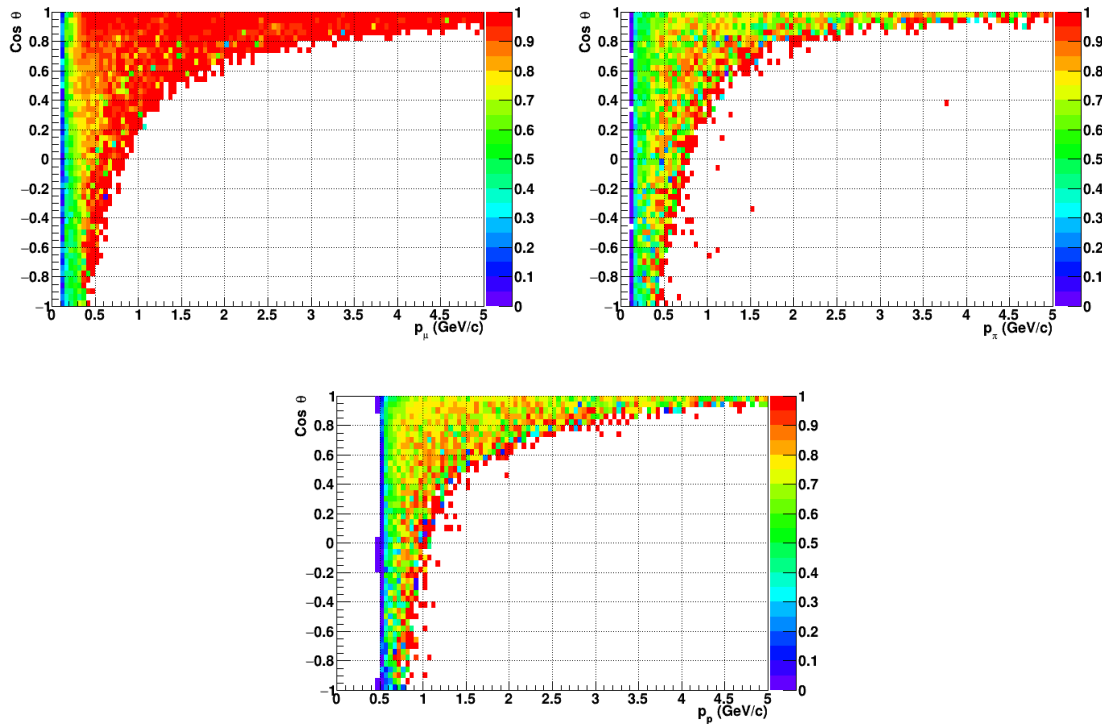


Figure 35: Reconstruction efficiency of muons (left), charged pions (right) and protons (bottom) in the WAGASCI water-module as a function of the particles momenta and angles.

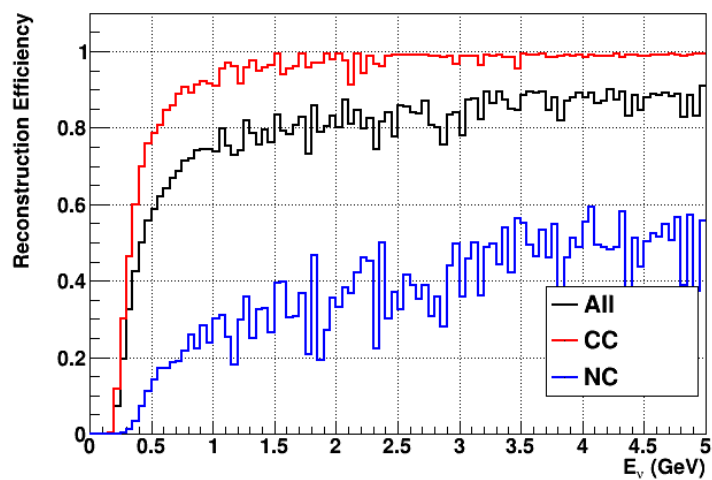


Figure 36: Reconstruction efficiency of all neutrino (black), CC (red) and NC (blue) interactions in the WAGASCI water-module as a function of the neutrino energy.

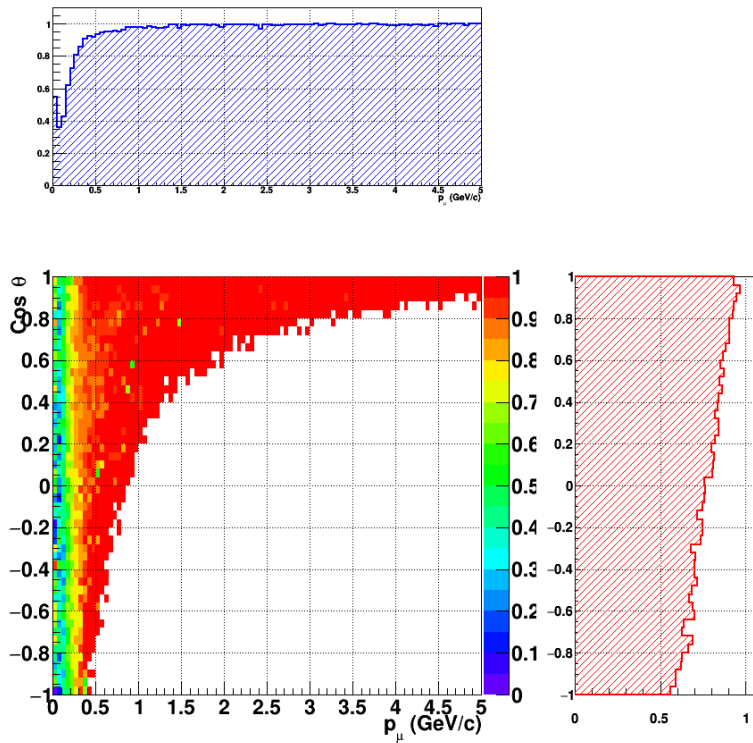


Figure 37: Reconstruction efficiency of CC interactions in the WAGASCI water-module as a function of the muon kinematic variables (momentum and angle).

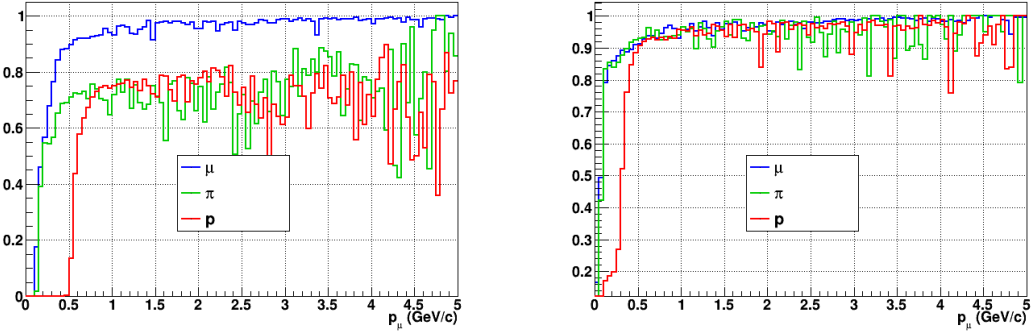


Figure 38: Reconstruction efficiency for muons, pions and protons in the water-in (left) and water-out (right) modules.

625 Note that a Particle Identification Algorithm has been also developed. It is based on
 626 the charge deposition of the particles in the scintillator, of the detection of a decay-electron.
 627 However, this information highly depends on the number of scintillator hit by a particle,
 628 which creates an important difference between a real WAGASCI module and the one used
 629 for the ND280-upgrade simulation. For this reason, the corresponding results will not be
 630 detailed here, but can be found in [?].

631 6.2 Background subtraction: the water-out module

632 In the nominal configuration, 20% of the neutrino interactions occurs on scintillators
 633 (C_8H_8). This background should be removed in order to measure the neutrino interac-
 634 tion on the same target as Super-K, which suppress the differences in cross-section models.
 635 For this purpose, we propose to use a water-out module, where the water is replaced by
 636 air. The detector is therefore fully active and has a 3 mm spatial resolution (scintillator
 637 thickness) which create an ideal detector to reconstruct and identify hadrons, and study
 638 np-nh interactions. The counter-part is the difference in particle energy deposition between
 639 the water and this water-out module that will need to be corrected for. In this section,
 640 we present the capabilities of such a module, and the impact it can have on cross-section
 641 measurements for the neutrino community in general and T2K in particular.
 642 The same reconstruction and selection as the water-in module is applied. Figure 38 shows
 643 the comparison between the water-in and the water-out reconstruction efficiencies for muon,
 644 pions and protons. 90% of the muons and 87% of the pions are reconstructed, while 70%
 645 of the protons are even reconstructed. It allows to lower down the proton threshold to
 646 250 MeV/c (see Table 9).

647 As a consequence of tracking even low momenta particle, the reconstruction efficiency
 648 is uniform and almost maximal on the entire $\cos \theta_\mu$ phase space, as shown on Figure 39.

	μ	π	p
Reconstruction Efficiency Momentum threshold	90% 50 MeV/c	87% 50 MeV/c	70% 250 MeV/c

Table 9: Reconstruction efficiency, proportions of μ -like and non μ -like and momentum threshold for muons, pions and protons in the empty module. The threshold is defined as the maximal momentum for which particles have a reconstruction efficiency smaller than 20%.

649 Since the fiducial mass represents 0.25 tons, the total number of events is divided by a
 650 factor of 3 compared to the water-in module. The water-out module offers interesting
 651 possibilities to study np-nh interaction since 70% of the protons are reconstructed. In the
 652 future, a possible separation as a function of the number of proton track will be studied.
 653 Moreover, we are currently pursuing the use of single and double transverse variables (cite
 654 Xianguo) to open new possibilities for separating np-nh from Final State Interactions, or
 655 for isolating the interactions on hydrogen from interactions on carbon in this module.

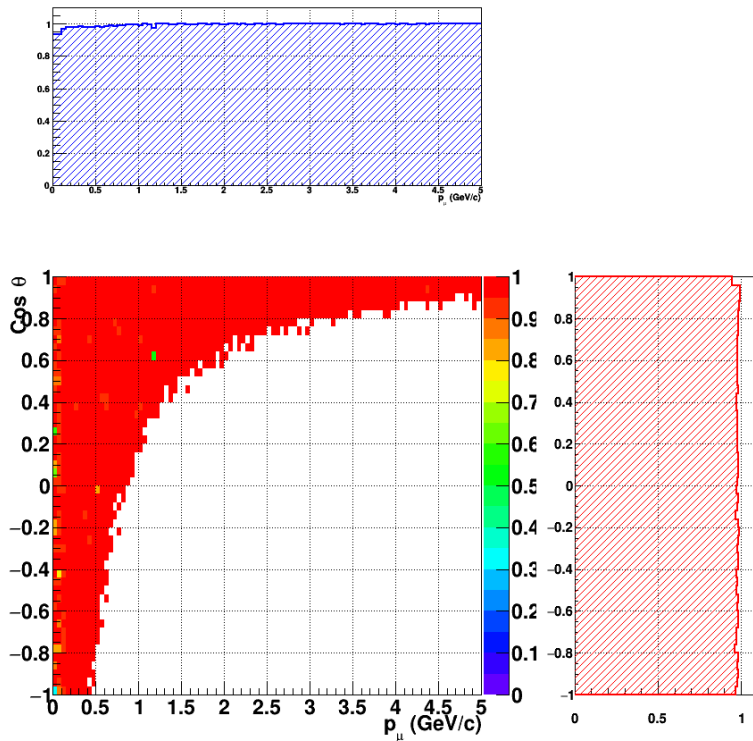


Figure 39: Reconstruction efficiency of CC interactions in the WAGASCI empty module as a function of the muon kinematic variables (momentum and angle).

656 **7 Schedule**

657 We would like to start a physics data taking from T2K beam time after the summer
658 shutdown in 2018. By then, commissioning and tests of the detectors will be completed
659 in J-PARC T59. The experiment can run parasitically with T2K, therefore we request no
660 dedicated beam time nor beam condition as discussed in the following section.

661 Once the approved POT is accumulated, the WAGASCI modules will be removed
662 from the experimental site, but we would like to keep the Baby-MIND and the Side-MRD
663 modules on the B2 floor of the NM pit as common platforms of future neutrino experiments
664 using the T2K neutrino beam.

665 **8 Requests**

666 **8.1 Neutrino beam**

667 The experiment can run parasitically with T2K, therefore we request no dedicated beam
668 time nor beam condition. As data taking periods, we request the ‘nominal’ T2K one-year
669 operation both for the neutrino beam and the antineutrino beam. The T2K has been
670 requesting 0.9×10^{21} POT/year and actually accumulating about 0.7×10^{21} POT/year in
671 recent years. For each year, starting from the Autumn, T2K is running predominantly in
672 the neutrino mode or in the antineutrino mode. Our request is to have one-year neutrino-
673 mode data and another one-year antineutrino mode data assuming that the POT for the
674 fast extraction in each year is more than 0.5×10^{21} POT.

675 **8.2 Equipment request including power line**

676 We request the followings in terms of equipment on the B2 floor:

- 677 • Site for the WAGASCI modules, Side-MRD modules and BabyMIND and their elec-
678 tronics system on the B2 floor of the near detector hall (Fig. 3).
- 679 • Anchor points (holes) on the B2 floor to secure the WAGASCI modules, Side-MRD
680 module and Baby-MIND (Fig. ??)
- 681 • Power line for the magnets in Baby-MIND: 400 V tri-phase 48-to-62 Hz, capable of
682 delivering 12 kW.
- 683 • Electricity for electronics and water circulation system, 3 kW, standard Japanese
684 electrical sockets.
 - 685 1. Online PCs: 2.1 kW
 - 686 2. Electronics: 0.7 kW
 - 687 3. Water sensors: ?

- 688 • Air conditioner for cooling heat generation at Baby-MIND magnets, online PCs and
689 electronics
- 690 • Beam timing signal and spill information
- 691 • Network connection

692 **8.2.1 Baby MIND Equipment request including power line**

693 We request the following in terms of equipment on the B2 floor:

- 694 • Site for the Baby MIND detector and its electronics systems on the B2 floor of the
695 near detector hall.
- 696 • Anchor points (holes) on the B2 floor to secure the 9 support frames, of order 4 holes
697 per frame, detailed floor plans to be communicated in a separate document.
- 698 • Power line for the magnet: 400 V tri-phase 48-to-62 Hz, capable of delivering 12
699 kW. We have a wish for the magnet power line to be installed and available to us by
700 beginning of March 2018.
- 701 • Electricity for electronics, 1 kW, standard Japanese electrical sockets.
- 702 • Beam timing signal and spill information
- 703 • Network connection

704 The infrastructure for much of the above exists already, and will be shared in part with
705 the WAGASCI experiment. Exceptions are the power line for the magnet and holes in the
706 B2 floor to anchor the detector support structures.

707 **9 Conclusion**

708 **References**

- 709 [1] K. Abe et al. Measurement of the muon neutrino inclusive charged-current cross sec-
710 tion in the energy range of 13 GeV with the T2K INGRID detector. *Phys. Rev.*,
711 D93(7):072002, 2016.
- 712 [2] M. Antonova et al. Baby MIND Experiment Construction Status. In *Prospects in*
713 *Neutrino Physics (NuPhys2016) London, London, United Kingdom, December 12-14,*
714 2016, 2017.
- 715 [3] K. Nitta et al. The k2k scibar detector. *Nucl. Instrum. Meth. A*, 535:147, 2004.

- 716 [4] J. Fleury, S. Callier, C. de La Taille, N. Seguin, D. Thienpont, F. Dulucq, S. Ahmad,
717 and G. Martin. Petiroc and Citiroc: front-end ASICs for SiPM read-out and ToF
718 applications. *JINST*, 9:C01049, 2014.
- 719 [5] M. B. Barbaro J. A. Caballero T. W. Donnelly G. D. Megias, J. E. Amaro. Inclusive
720 electron scattering within the susav2 meson-exchange current approach. *Phys. Rev. D*,
721 94:013012, 2016.
- 722 [6] Yu. G. Kudenko, L. S. Littenberg, V. A. Mayatsky, O. V. Mineev, and N. V. Ershov.
723 Extruded plastic counters with WLS fiber readout. *Nucl. Instrum. Meth.*, A469:340–
724 346, 2001.
- 725 [7] O. Mineev, Yu. Kudenko, Yu. Musienko, I. Polyansky, and N. Yershov. Scintillator
726 detectors with long WLS fibers and multi-pixel photodiodes. *JINST*, 6:P12004, 2011.
- 727 [8] Etam Noah et al. Readout scheme for the Baby-MIND detector. *PoS*, Pho-
728 toDet2015:031, 2016.